batteries

MDPI

Review

A Review on Recent Progress Achieved in Boron Carbon Nitride Nanomaterials for Supercapacitor Applications

Feng Liu [1], Xiang Zhao [2], Ping Shi [1], Laishi Li [1], Qidi Dong [1], Mi Tian [3], Yusheng Wu [1,*] and Xudong Sun [4,*]

[1] School of Materials Science and Engineering, Shenyang University of Technology, Shenyang 110870, China; lffengliulf@sut.edu.cn (F.L.); lilaishi@sut.edu.cn (L.L.)
[2] Institute of Innovative Science and Technology, Shenyang University, Shenyang 110003, China
[3] Trubon Construction Technology (Shenzhen) Co., Ltd., Shenzhen 518101, China
[4] Foshan Graduate School of Innovation, Northeastern University, Foshan 528311, China
* Correspondence: wuyus@sut.edu.cn (Y.W.); xdsun@mail.neu.edu.cn (X.S.)

Abstract: Supercapacitors are regarded as reliable energy storage devices to alleviate the energy crisis and environmental pollution. However, the relatively low capacitance and low energy density limit the practical application of supercapacitors. In this context, boron carbon nitride (BCN) nanomaterials have been extensively studied in the past decade due to their chemical and thermal stability, high mechanical strength, as well as tunable bandgap. The specific capacitance and energy density of supercapacitors can be significantly improved by fabricating nanostructured BCN-based electrode materials. In this review, the recent advances in the application of BCN-based materials in supercapacitors is presented. Strategies such as structure design, porosity/defect engineering, and hybrid nanostructure construction to boost the electrochemical performance of BCN-based materials are provided and, finally, promising research directions for novel energy storage materials are proposed.

Keywords: boron carbon nitride; h-BN; supercapacitor; nanomaterials; energy storage

Citation: Liu, F.; Zhao, X.; Shi, P.; Li, L.; Dong, Q.; Tian, M.; Wu, Y.; Sun, X. A Review on Recent Progress Achieved in Boron Carbon Nitride Nanomaterials for Supercapacitor Applications. *Batteries* **2023**, *9*, 396. https://doi.org/10.3390/batteries9080396

Academic Editor: Peter Mahon

Received: 6 June 2023
Revised: 18 July 2023
Accepted: 28 July 2023
Published: 30 July 2023

1. Introduction

The massive use of traditional fossil energy has caused serious environmental pollution and the growing energy crisis, which has urged mankind to transition to sustainable energy sources instead of fossil fuels [1]. In order to solve these issues, electrical energy is gaining major popularity because it can be generated through clean and renewable resources such as solar, biomass, tidal, and wind energy. Electrical energy as an energy carrier can provide great potential to increase the sustainability of human beings' lives. However, the problem with electricity is the lack of a stable energy storage mechanism to store excess energy during the night trough period. In this regard, rechargeable batteries and supercapacitors (SCs) are emerging as effective storage media. As compared to batteries, SCs have a lower energy density but possess high power density, are eco-friendly, have a quick charge–discharge capability, stable recyclability, a relatively low cost, and higher safety [2]. It is promising for SCs to replace batteries as SCs can bridge the gap between rechargeable batteries and electrolytic capacitors in terms of their electrochemical properties.

Unlike batteries, SCs store energy through kinetically faster physisorption of charges or (near) surface-confined faradaic reactions of electrodes [3]. According to their charge storage behavior, SCs can be divided into three types: electrochemical double-layer capacitors (EDLCs), electrochemical pseudocapacitors, and hybrid supercapacitors [4]. EDLCs stores charges at the "Helmholtz layer" formed through electrostatic interactions between the electrode/electrolyte interface, while a pseudocapacitor works using the faradaic process (or redox reaction) on the electrode (near) surface [5,6]. The charge storage mechanism of a hybrid supercapacitor is based on both faradaic and non-faradaic processes. Although the three types of SCs have different energy storage mechanisms, the type and mechanism of the SCs all directly depend on the performance of the electrode materials. Hence, it

is urgent and necessary to develop advanced electrode materials with greater capacity, voltage, and energy densities for future SCs.

In the past decades, a number of researchers have been preparing advanced materials and hybrid composites with specific architectures and nano-dimensional structures to improve the electrochemical performance of SCs [7,8]. It is not surprising that two-dimensional (2D) materials such as graphene, hexagonal boron nitride (h-BN), graphitic carbon nitride (g-C_3N_4), transition metal dichalcogenides (TMDs), metal oxides and hydroxides, covalent organic frameworks, and MXene, etc., are widely used in capacitor fabrication [9–11]. The unique structure, large surface area, reactive basal planes or edges, interlayer spacing, tunable thickness, and composition make 2D materials highly appealing compared to bulk materials to accommodate faradaic reactions and insertion pseudocapacitance [12]. However, wide bandgap 2D materials such as g-C_3N_4 and h-BN often suffer low electrochemical performance, including inferior energy density, insufficient capacity, low volumetric capacitance, low conductivity/stability during electrode reaction, and smaller operating voltage when they are used in supercapacitor applications [10,13–16]. To overcome these challenging issues, an emerging material named boron carbon nitride (BCN) has attracted extensive attention for application in SCs [17,18].

Boron carbon nitrides (BxCyNz) are ternary compounds with diverse compositions and various applications in supercapacitors, electrocatalysis, CO_2 photoreduction, wastewater treatment, hydrogen production, and several others [19–21]. Such BxCyNz species would combine the unique properties of graphene and h-BN with adjustable properties depending on element portion and structure [22]. As compared to other applications, the amalgamation of graphene and BN-type structures permits BCN to adjust its electronic properties as required for SC applications. Heteroatom doping makes BCN possess an enhanced electrical conductivity, more active sites, and improved surface charge mobility and wettability compared to carbon and h-BN materials. Therefore, BCN materials show great promise in SC applications.

Recently, several review papers on the synthesis and applications of h-BN and BCN, such as photocatalysis, wastewater treatment, electrocatalysis, and energy storage devices, have appeared [23–26]. For example, Han et al. surveyed the research work on functionalized h-BN and its energy-related applications such as electrocatalysis, hydrogen storage, catalytic dehydrogenation reaction, and batteries [19]. Recepoglu et al. summarized the preparation methods such as chemical vapor deposition (CVD), magnetron sputtering, and ion-beam-aided deposition, as well as several environment applications of 2D BCN materials [24]. These articles either focus on the fundamental properties and various applications of BCNs or emphasize the diverse synthesis techniques, growth, and characteristics of thin BCN films [27]. However, there is hardly any review only concentrated on the SC application of BCN nanomaterials. Although the research on the utilization of BCNs for SCs is still in its infancy, a comprehensive review of published works is needed to summarize recent advances in the field of materials science with the rapid growth of BCN research. In order to overcome the challenges of applying BCNs in SCs, strategies are needed to prepare BCN nanomaterials with controllable morphology and electronic structure, thus tuning the insulating properties of h-BN to semiconducting or conducting properties. Modification strategies are also needed to boost the electrochemical performance of BCN. Therefore, it is crucial to sum up the achievements of BCN-based electrode materials along with their development and future aspects.

This paper provides a summary of the exceptional contribution of BCN nanomaterials in supercapacitor applications. The recent studies directed towards the design, synthesis, and characterization of BxCyNz containing hexagonal BCN networks are presented. This work mainly focuses on the understanding of the relationship between BCNs' chemical composition, morphology, and hybrid structures with their electrochemical performance in SCs. The challenges to boost the electrochemical performance of BCN electrode materials have been considered and modification strategies to bypass the drawbacks have been

provided. The goal of this review is to facilitate the design of high-performance BCN electrode materials for future energy storage systems.

2. Definition and Properties of Boron Carbon Nitride

Owing to the reciprocal electron structure and similar atomic size among the B, C, and N elements, each two of them can form a stable covalent bond [28]. In order to understand the compositional diagram of the BxCyNz materials, Figure 1 exhibits a phase illustration of different layered hexagonal phases via the combination of these three elements. Each corner at the intersection of a triangle and a circle represents a pure phase. For example, graphene is considered in the C corner while 2D borophene is regarded at B. Boron-doped carbon, such as B_4C, BC_3, and other metastable intermediate phases will be produced when moving towards boron from C. Similarly, nitrogen-doped carbon such as C_3N_4 and C_3N_5 will be observed between the C and N corners. Along the B–N side, the middle point represents cubic or hexagonal BN. It is worth noting that diamond, B_4C and c-BN are sp^3 hybridized as super hard materials, while graphene, graphitic-C_3N_4, and h-BN have sp^2 configurations and are known as 2D substances. The sp^3 hybridized B-C regions may disrupt the 2D configuration desired for a BCN material [18]. Through well-controlling the thickness and composition of B, C and N, the 2D h-BCN material would be formed at the center point of the diagram.

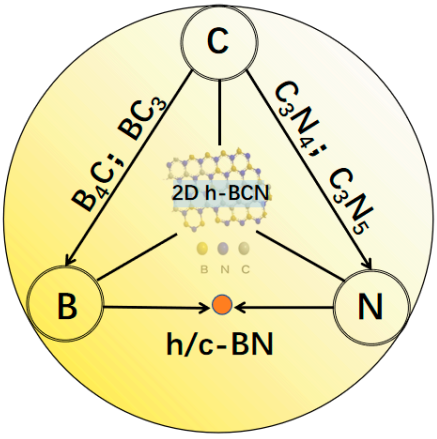

Figure 1. Phase diagram of BxCyNz materials formed by different stoichiometries among B, C, and N elements.

Depending on the stoichiometry of B, N, and C, a number of hybridized and randomly distributed h-BN and graphene domains (BxCyNz system, $0 \leq x, y, z \leq 1$) can be formed with constitutions varied, from pure h-BN to pure graphene, as shown in Figure 2a [29]. As depicted in Figure 2b, pure graphene is a zero-bandgap material while wide-bandgap h-BN can be regarded as an insulator [30]. Considering the similar honeycomb structure of graphene and h-BN, h-BCN material not only inherits the excellent chemical and thermal stabilities of h-BN, but also possesses a smaller band gap and improved electrical conductivity due to the carbon doping. Through adjusting the arrangement and atomic ratios of B, C, and N atoms, the optical, mechanical, magnetic, and electrical properties of BxCyNz materials can be easily tuned [31,32]. As a hybrid phase of h-BN and graphene, BCN semiconductors offer a tunable bandgap and stronger charge carrier mobility than insulated h-BN [32]. At the same time, doping h-BN domains gives BCN a higher oxidation resistance than graphene [33]. Relying on the unique planar structure, large specific surface area (SSA), high electrical and thermal conductivity, and easily controlled components and thicknesses, BCN exhibits tremendous potential in supercapacitor applications.

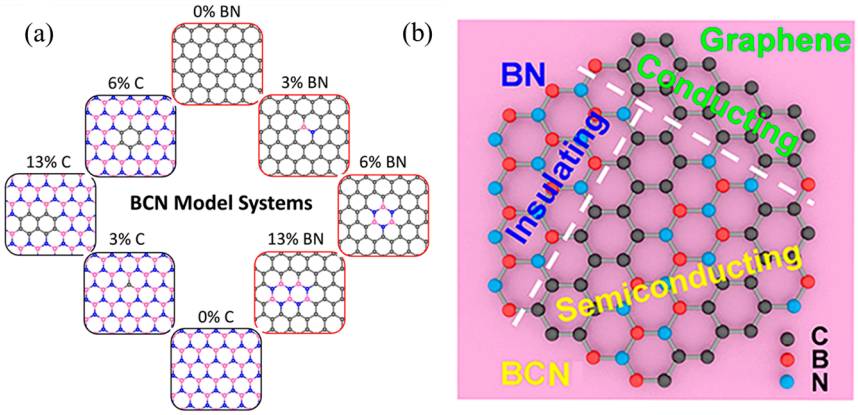

Figure 2. (**a**) Schematic of the BCN configuration models. Gray, blue, and pink atoms are defined as C, N, and B, respectively. %X components indicates the ratio of the number of substituted C/BN pairs in h-BN/graphene substrate. Reprinted with permission from [29]. Copyright 2020, American Chemical Society. (**b**) Schematic illustration of the hybridized nanocrystal composition of the 2D h-BC_2N film. Reprinted with permission from [30]. Copyright 2020, American Chemical Society.

However, it is difficult for BCN materials to achieve the good control of composition and dimensionality in all circumstances. The final B:C:N ratio and nanostructure will determine the physical and chemical properties of the BxCyNz material. In general, varying the atomic ratio and controlling the shape and size of BCN nanomaterials may pave the way to innovative and intriguing electrode materials.

3. Synthesis of Nanostructured BCN Materials

Low-dimensional BCN nanomaterials exhibit interfacial effects and quantum confinement with unique properties compared with bulk BCN materials. To date, noteworthy attempts have been reported for the preparation of BCN materials with related nanostructures such as zero-dimensional (0D) quantum dots, one-dimensional (1D) nanotube/nanorods, 2D nanosheets, and three-dimensional (3D) aerogels or foams, mainly employing techniques such as chemical vapor deposition (CVD), pyrolysis, and solvothermal/hydrothermal methods. These approaches use either single or different sources for B, C, and N precursors, which are briefly summarized in the following subsections.

3.1. Chemical Vapor Deposition

CVD is one of the most common methods in which 2D materials such as graphene are formed by gaseous substances reacting on the substrate surface or in the gas phase. Kaner et al. reported one of the earliest syntheses of graphitic BCN films by thermal decomposition of boron trichloride, ammonia, and acetylene at 400–700 °C in 1987 [34]. Since then, diverse modified CVD processes have been proposed to prepare B-C-N ternary materials, i.e., ambient pressure CVD (APCVD), low-pressure CVD (LPCVD), microwave plasma CVD (MPCVD), laser CVD (LCVD), and plasma-enhanced CVD (PECVD) [27,35–37]. Varying CVD experimental parameters such as temperature, time, buffer gas, precursor and substrate selection, and distance between the source and the substrate can control the layer structure, thickness, micro-size, and orientation of the BCN material [38]. Yang et al. fabricated a graphene/h-BN heterostructure using PECVD in which large-area graphene single crystals with a fixed stacking orientation were successfully grown [39]. Tang et al. subsequently realized a growth of micron-sized graphene domains on an h-BN substrate via a gaseous silane catalyst-assisted CVD [40]. Ultra-flat h-BN has emerged as an ideal substrate for graphene nanodevices and shows promise to engineer graphene's electronic structure. Kim et al. recently reported a facile CVD method using a single molecular precursor, N-tri-methyl borazine, to prepare h-BxCyNz films on a Ni catalyst [41]. The atomic structure of the product closely resembles h-BC_2N and the bandgap decreased to 2.15 eV by arranging the B, C, and N atoms in an sp^2 network. The obtained h-BC_2N films exhibited photoluminescence and electroluminescence as potential

candidates for 2D light-emitting diode applications. Recently, Yi et al. successfully grew a 2D hybridized BC_2N film with a band gap of about 2.3 eV through the PECVD method [30]. The mechanism of the temperature-dependent PECVD growth is illustrated in Figure 3.

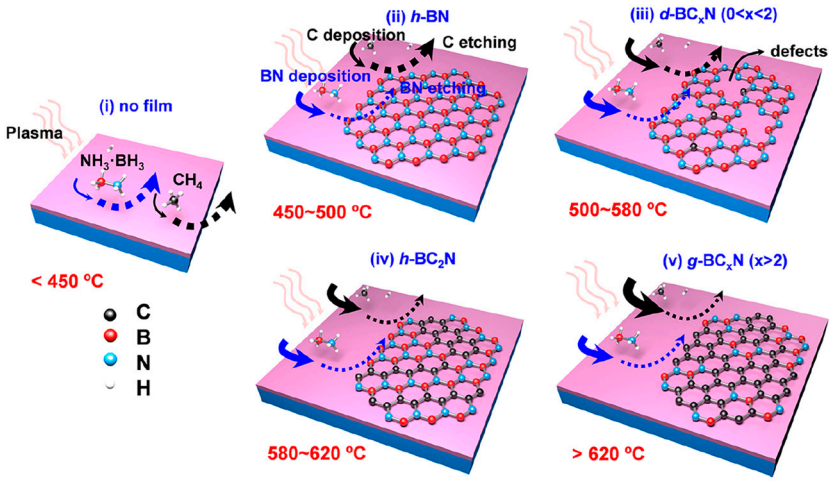

Figure 3. Schematic illustration of the growth of BxCyNz products via PECVD at different temperatures. Reprinted with permission from [30]. Copyright 2020, American Chemical Society.

Above 500 °C, C atoms begin to deposit while the plasma will etch and remove some C atoms, leading to the formation of a defective BCxN film. At 580–620 °C, deposition and etching reach a relative equilibrium, resulting in the growth of h-BC_2N. When the reaction temperature is over 650 °C, C deposition and nucleation dominate and eventually produce a thick graphitic BC_2N film. Over the years, CVD has become a preferred technique for the growth of high-quality BCN films with controlled defect sites and lateral sizes.

3.2. Pyrolysis

The advantages of CVD methods for preparing h-BCN lie in the simple preparation principle and the ability to obtain large layered h-BCN single crystals. However, its disadvantages include poor controllability of the reaction process, complicated operation, high cost, and unsuitability for industrial production. Compared with CVD, the pyrolysis method has the advantages of low cost, simplicity, high yield, and can be used for large-scale industrial production. Through designing a special synthesis process, the composition, morphology, and size of the BCN product can be controlled. This subsection summarizes three categorized pyrolysis approaches.

3.2.1. Template-Assisted Methods

Due to the atomic similarity between B and C, nanostructured carbon materials with various morphologies can serve as a template to prepare BCN materials. The structural similarity between h-BN and graphite allows B and N atoms to replace C atoms on the carbon skeleton during the reaction. At high temperatures, the boron source decomposes into boron trioxide (B_2O_3) compounds, which react with nitrogen-containing gases (N_2, NH_3) and carbon, ultimately forming BCN. The following reactions are involved during the substitution:

$$2H_3BO_3 \rightarrow B_2O_3 + 3H_2O, \quad (1)$$

$$B_2O_3 + 5C + N_2 \rightarrow 2BCN + 3CO, \quad (2)$$

$$B_2O_3 + 2C + NH_3 \rightarrow 2BCN + 3H_2O, \quad (3)$$

As a carbon template, carbon nanotubes (CNTs), activated carbon, graphite, and carbon nanocages have been used for the preparation of BCN nanotubes (BCNNTs), BCN nanosheets (BCNNs) and BCN nanocages, respectively [42–47]. Luo and co-workers reported a bio-hydrogel template method to manufacture 3D BCN ceramic aerogels which possess improved crystallinity, increased SSA, and enhanced photocatalytic performance [48]. Similarly, graphitic carbon nitride (g-C_3N_4) also offers an excellent platform to synthesize BCNNs with various ratios of B, C, and N. Portehault et al. obtained nano- and mesoporous BCN materials with high SSA, up to 1560 $m^2\ g^{-1}$, by using the mesoporous g-C_3N_4 as a hard template and BH_3-$NH_2{}^tBu$ as the boron source [49]. Wang et al. used g-C_3N_4 as a sacrificial template and boric acid (H_3BO_3) as the boron source to control the formation of BCNNs [50]. The specific capacitance of the BCN product is 134.5 F g^{-1}, which is greater than the 47.2 F g^{-1} value of g-C_3N_4/G nanosheets at a scan rate of 5 mV s^{-1}. Li et al. produced a series of flake-like BCNNs by calcinating H_3BO_3 and g-C_3N_4 at different reaction temperatures [51]. As shown in Figure 4, g-C_3N_4 is both implemented as a carbon source and nitrogen source. C atoms are gradually substituted by B with the increasing temperature. The carbon content decreased to 9.67 at% of BCN-800 (prepared at 800 °C) from 25.33 at% of BCN-600. In addition, other templates of boron and nitrogen-containing frameworks, metal−organic frameworks (MOFs), ionic liquids, and mesoporous molecular sieves have also been used [52–54]. For example, Goyal et al. manufactured a hierarchical porous BxCN material from a dimethylaminoborane precursor and an SBA-15 template [55]. BCN products can successfully replicate the porous structure of templates via this method. However, the relatively complex preparation process and the difficulty of completely removing the template also limit the application of template-assisted approaches.

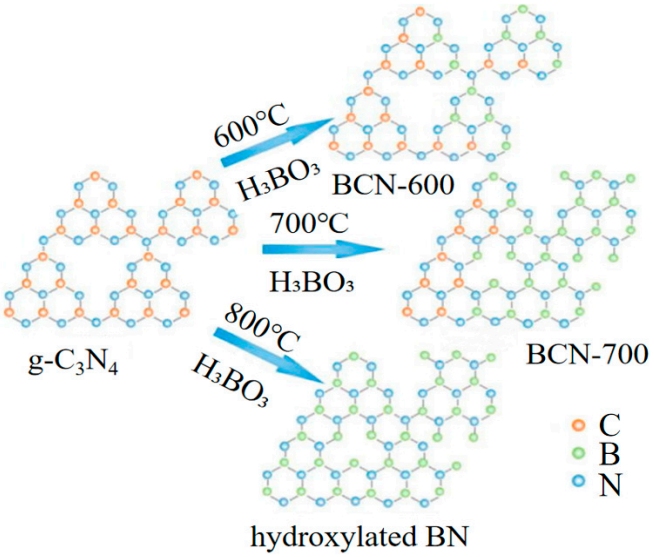

Figure 4. Schematic illustration of g-C_3N_4 template-assisted approach for the preparation of BCN. Reprinted with permission from [51]. Copyright 2017, Elsevier.

3.2.2. Precursor Pyrolytic Methods

Template-assisted methods often suffer the disadvantages of insufficient filling of precursors, sophisticated and harmful template removal steps, a long synthesis time, and high cost, which hinder their large-scale application. Conversely, template-free pyrolysis is currently the most common and scalable method for synthesizing h-BCN. By simply adjusting the synthesis process and changing reaction parameters such as temperature, time, gas flow, and the B:C:N precursor ratio, the morphology, structure, and size of the BxCyNz products can be regulated. For the high-temperature pyrolysis method, precursor selection plays a vital role in deciding the final morphologies and properties of the BCNs. Massimi et al. fabricated a ternary nanocrystalline BCN compound by using a single molecular precursor, ethane 1,2-diamineborane [56]. The initial B:C:N ratio of the raw material

was 1:1:1, while the BCN product presented a 0.11:0.76:0.13 stoichiometry, richer in C–C networks with respect to the bulk. Zhang et al. successfully synthesized crystalline BC_2N quantum dots (QDs) with high yield by in situ two-step thermal decomposition of a single sodium cyanoborohydride precursor in a hydrogen-rich environment [57]. Liu et al. reported a synthesis of BCN nanorods using two easily accessible precursors with melamine as a carbon and nitrogen source and H_3BO_3 as a boron source [31]. Through controlling the carbon content via a simple oxidation process, BCN compounds exhibit colorful fluorescence properties under ultraviolet (UV) excitation. Giusto et. fabricated sp^2-conjugated B-C-N films from a simple solid precursor pyrolytic method at a lower temperature [58]. Through the thermal polymerization of a melamine and H_3BO_3 mixture at 550 °C, the as-prepared thin BCN films showed tunable energy levels and band gaps with a near-UV up to 460 nm photoluminescence emission via tuning the precursor content. Han et al. demonstrated that a two-step reaction could be used to produce C-doped h-BNNS with the usage of ammonia borane and ethylenediamine [59]. Figure 5a depicts the synthetic route in which a polymeric precursor is firstly produced and then the BN nanosheet is formed with uniformly dispersed carbon atomic clusters. Electron microscopic characterization results (Figure 5b–g) indicate that h-BCN has a sheet-like morphology and sp^2 hybridized B-C-N structure. Electron energy loss spectroscopy (EELS) mapping confirms that C atoms are distributed in small atomic clusters throughout the h-BN framework.

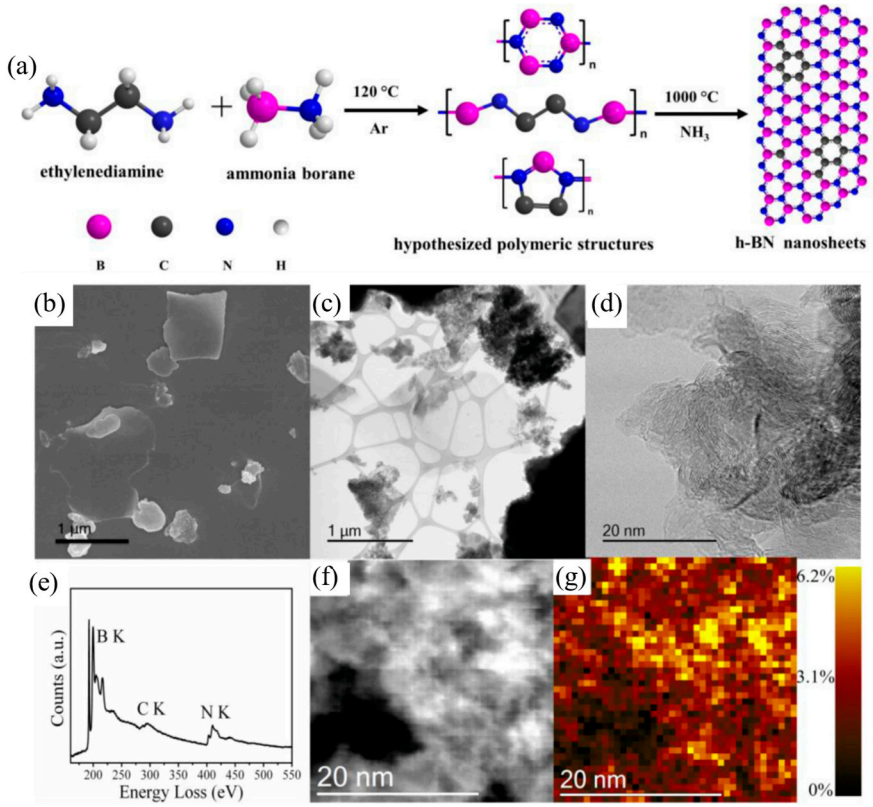

Figure 5. (**a**) Schematic illustration of the template-free synthesis of h-BCN nanosheets, (**b**) SEM image, (**c**) STEM image, (**d**) high-resolution STEM images of h-BCN, (**e**) EELS spectrum of h-BCN, (**f**,**g**) EELS mapping of carbon with a spot size of 0.75 nm × 0.75 nm. Reprinted with permission from [59]. Copyright 2021, Elsevier.

Except for the above precursors, it is more common to introduce an extra carbon source to finely manipulate the composition of BCN products [60]. In general, BCN can be obtained from the thermal transformation of B, C, and N precursors at high temperatures. For example, Huang et al. reported a synthesis of semiconducting BCN materials via the thermal decomposition of H_3BO_3, urea, and glucose mixtures at 1250 °C for 5 h [61]. The

as-prepared products showed promise in catalyzing H_2 or O_2 evolution from water as well as CO_2 reduction under visible light irradiation. Wang et al. acquired a highly porous BCNNS via the thermal pyrolysis of poly(ethylene oxide-co-propylene oxide) (p123) and a polymeric gel precursor which was formed by hydroxyl and amino group cross-linking between polyvinylic alcohol (PVA), H_3BO_3, and guanidine carbonate [62]. The BCNNS products had a surface area of up to 817 m^2 g^{-1} and exhibited a comparative oxygen reduction reaction (ORR) performance to commercial Pt/C and carbon materials in both alkaline and acidic solutions. Zou et al. developed an effective synthetic approach for BCNNTs via the assembly and pyrolysis of H_3BO_3, urea, and polyethylene glycol (PEG) [63,64]. It was found that PEG-2000 favored the formation of BCNNTs with segregated B–C and N–C bonds. Compared to commercial Pt/C catalysts, BCNNT products exhibit size-dependent ORR performance with Pt-like ORR activity and superior ORR stability. Zhang et al. subsequently used a similar method to prepare BCNNTs which were considered as ideal platform catalysts to clarify the origin of the activity, similarity, and difference of nonmetallic carbon and BN materials [65]. The B, C, and N contents of BCNNTs can be regulated in a wide range by varying the PEG precursor content, while the O content of BCNNTs can be regulated via a low-temperature oxidation in air. BCNNT catalysts show an enhanced methanol conversion of 29% and high selectivity to formaldehyde which is up to 54%. Hence, the precursor pyrolytic method is becoming a prevalent process for nanostructured BCN synthesis because it is stable, cost-effective, and is easy to expand in scale to meet industrial production requirements.

3.2.3. Molten Salt Synthesis

Molten salt synthesis (MSS) is another widely used method to prepare BN-based nanomaterials [66–68]. As illustrated in Figure 6, the precursor will be converted to BCN in melting salt and eventually form different products such as nanosheets or nanoparticles after removing the solid salts. The salt melting point, precursor solubility, and system stability are extremely important factors which will influence the reaction rate, particle size, and surface morphology of the BCN product. Lei et al. reported a facile synthesis of BCN nanoparticles in a eutectic LiCl/KCl salt melt with the usage of sodium borohydride and guanidine raw materials [69]. Relying on the LiCl/KCl melting salt, the reaction temperature decreased to 700 °C without any other post-treatment and harsh experimental conditions compared to CVD and pyrolysis processes. Liu et al. quickly obtained a thin BCNNS product from a single molecular precursor ethylenediamine bisborane (EDAB) at 1000 °C via MSS [33]. During the synthesis, a liquid reaction environment forms from the KCl/NaCl melting salt which will accelerate the dissolution of precursor molecules and prevent the self-agglomeration of BCN layers. For high-temperature pyrolytic treatment, bulk BCN products are quite often acquired after the pyrolysis of B, C, and N precursors. Instead, MSS tends to favor the formation of thin 2D BCNNS because of the rapid mass transport and quick solvation of the precursor molecules in the liquid melting salt environment [70–72]. Jing et al. utilized H_3BO_3, tripolycyanamide (N source), and PEG as the precursors to produce boron carbon oxynitride (BCNO) nanosheets at 750 °C through the KCl/NaCl molten-salt-assisted method [73]. Zhang et al. attained atomically thin BCNNS through decomposing boron oxide, melamine, and glucose mixtures in a KCl/NaCl salt melt at 1250 °C for 5 h [74]. Compared with the bulk BCN material prepared by the direct pyrolysis of precursor mixtures, the semiconducting BCNNS which are prepared via the molten-salt-assisted assembly growth strategy have atomic-level thickness (0.4 nm), micron lateral size (~10 μm), and enhanced photocatalytic activity for H_2 evolution. Wang et al. subsequently investigated the effects of molten salt type and carbon content on the formation of BCNNS using the same starting materials [75]. It was found that LiCl-KCl melting salt was more favorable than NaCl-KCl as a liquid melting medium for the growth of BCNNs. This is because the lower melting point of LiCl-KCl (353 °C) compared to NaCl-KCl (657 °C) is conducive to quicker BCN formation in a liquid environment. Furthermore, the higher average electronegativity of cations in the melting LiCl-KCl salt can provide

higher solubilities for the formed B and N intermediates. When the C content increases to 40% (molar ratio), the obtained $BC_{0.4}N$ products have a sheet-like morphology of about 10 nm thick and an SSA as high as 484 m^2 g^{-1}. To conclude, the swift solvation and accelerated mass transfer of the reactants in melting salt are beneficial to the production of nanostructured BCN materials.

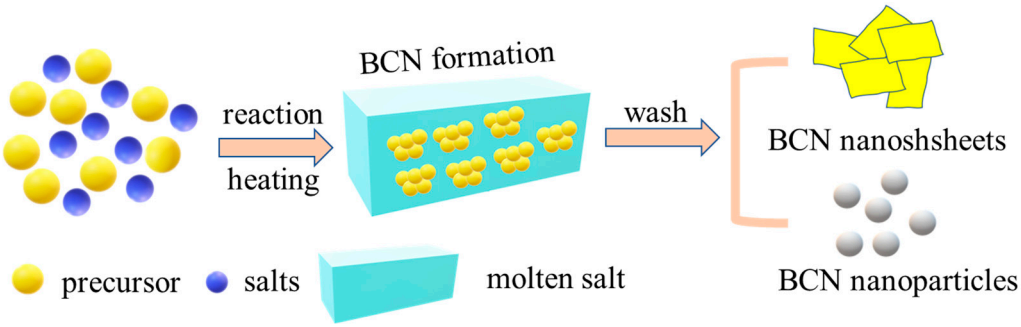

Figure 6. Schematic illustration of molten salt synthesis for the preparation of BCN.

3.3. Other Methods

A solvothermal method was used to prepare BCN materials with the utilization of different precursors. Huang et al. reported that a solvothermal reaction of $CH_3CN{\cdot}BCl_3$ and lithium nitride using benzene as the solvent had been successfully applied in the synthesis of BCN phases at 300 °C and less than about 7 MPa [76]. Wang et al. fabricated three different BCNNs with tuned C contents (5.5–14.3%), SSA (82–290 m^2 g^{-1}), and morphologies (ultrathin nanosheets, triangular plates) by using ammonium fluoroborate ($NaBH_4$), sodium azide (NaN_3), and alcohol as reactants at different temperatures. This work demonstrates that BCNs are promising nonmetallic catalysts in dehydrogenation applications. BCNs could also be prepared through the chemical or mechanical exfoliation from a bulk material [10]. Shi et al. obtained large size (1–20 μm) and ultrathin (thickness of ≈1–3 nm) BCNNs with a complete lattice structure through a novel "ultrasonic ball milling" strategy [77]. This strategy achieved the synergistic utilization of shear force and friction force by adding moderate sapphire (Al_2O_3) abrasive in the liquid phase system, producing high-quality BCN materials. Interestingly, Li et al. utilized molten hydroxide to chemically exfoliate bulk h-BN in a top-down method [78]. During the reaction of h-BN and hydroxides, cations (Na^+ or K^+) and anions (OH^{-1}) are inserted into the interlayer gap of BN in self-curling nanosheets, ultimately promoting the detachment of BN sheets from the parent h-BN material. This method can be extended for efficient chemical stripping of BCNNs from bulk BCN materials [24].

Some selected BCN synthesis methods reported in the literature are summed up in Table 1. Among all the above-mentioned approaches, using CVD techniques to prepare BCN is limited due to the expensive substrate, high temperature and difficulty to operate. The solvothermal method and chemical or physical exfoliation are of high cost and may have toxic chemical effects [18]. The template-assisted method requires specific templates and a time-consuming removal process and is not a cost-effective approach. Precursor pyrolysis and MSS are relatively easier, less time-consuming, and more efficient to study the nano-structures and intrinsic properties of BCN materials at the atomic level. Through arranging the B, C, and N compositions, advanced nanostructures and desired products can be obtained via pyrolysis.

Table 1. Table highlighting the relevant literature on BCN synthesis parameters.

Method	Materials with Composition (B:C:N) in Atomic Ratio (%)	Precursor	Temperature (°C)	Properties of Products	Advantages/Disadvantages	Ref.
CVD	2D h-BC_2N (25:48:27)	$BH_3{\cdot}NH_3$, CH_4, SiO_2/Si substrate	580~620	• Band gap of about 2.3 eV, p-type conducting property	• Can produce high quality BCN films	[30]
	h-BxCyNz films	N-tri-methyl borazine	1000	• Bandgap decreased to 2.15 eV	• High cost; complicated operation	[41]
Template-assisted methods	3D BCN ceramic aerogels (55.5:10.7:30)	H_3BO_3, urea, starch, NaCl	1250	• 880 m^2 g^{-1}	• Replicate the porous structure of template	[48]
	BCNNs (16.09:58.77:10.72)	g-C_3N_4, H_3BO_3	900	• 330 m^2 g^{-1}	• Insufficient filling of precursors; sophisticated and harmful template removal steps	[50]
	Hierarchical BxCN (26.9:60.4:12.7)	Ethylenediamine, dimethylaminoborane,	600	• 620 m^2 g^{-1}		[55]
Precursor pyrolysis	BCN thin films (9.4:34:56.6)	Melamine, H_3BO_3	550	• Bandgap decreased to 2.71 eV	• Feasible, cost-effective, stable, and scalable	[58]
	BCNNs (42.5:8:39.5)	B_2O_3, glucose, urea	1250	• Bandgap of 2.72 eV, 520 m^2 g^{-1}	• Long-time synthesis at high temperature is sometimes adverse for the preparation of BCN nanomaterials	[61]
	BCNNs (11.48:76.02:12.5)	PVA, H_3BO_3, guanidine carbonate salt	900	• 817 m^2 g^{-1}		[62]
	BCNNT (16.16:66.2:15.06)	H_3BO_3, urea, PEG-2000	900	• 890 m^2 g^{-1}		[63]
Molten salt synthesis	BCNNS	EDAB, KCl-NaCl	1000	• Bandgap decreased to 1.90 eV	• Time-saving, green, and beneficial to prepare nanostructured BCN materials	[33]
	BCNO nanosheets	Tripolycyanamide, H_3BO_3, PEG, KCl-NaCl	750	• Lamellar structure with a thickness of ~5.8 nm		[73]
	BCNNS	B_2O_3, melamine, glucose, KCl-NaCl	1250	• Bandgap of 2.56–2.95 eV	• Small crystals, corrosion to furnace tubes	[74]
Solvothermal method	h-BCN phases (14.43:36.63:20.78)	$CH_3CN{\cdot}BCl_3$,Li_3N, benzene	300	• Hexagonal structures containing very small single crystals and polycrystalline	• Low temperature; can maintain complete lattice structure	[76]
Ultrasonic ball milling	BCNNS	Bulk BCN, Al_2O_3	30	• A lateral size of 1–20 μm and a thickness of 1–3 nm	• High cost and may have toxic chemical effects	[77]

4. Application of Boron Carbon Nitride in Supercapacitors

Carbon-based nanomaterials such as activated carbon, CNT, and graphene are extensively applied in energy conversion and storage while h-BN is rarely employed in electrochemical energy systems because of the wide bandgap and insulating nature of BN. However, h-BN can actually be used to alleviate the thermal deformation of conventional organic separators, weak solid electrolyte interface layers of metal anodes, and electrocatalyst poisoning in electrochemical systems due to its chemical and thermal stability, and high mechanical strength [9,79]. In recent years, BCN has come to be regarded as a promising electrode material for next generation SCs since it combines the excellent physicochemical properties of h-BN and graphene. A summary of the latest research on the application of BxCyNz materials for supercapacitors is presented in this section.

4.1. BN-Graphene Composite-Based Supercapacitor

Theoretical calculations and experimental studies have demonstrated that the composite of h-BN and graphene can be applied in SCs [15,16,80–84]. In recent years, h-BN has come to be regarded as an ideal candidate for fabricating van der Waals heterostructures when combining it with graphene due to its remarkable mechanical, thermal, and electronic properties [15,16,82–84]. This class of h-BN/graphene heterostructures can be tuned for exceptional properties such as regulating the intrinsic electronic structure of h-BN and enhancing the carrier mobility of graphene, or used for SCs [85]. Byun and co-workers utilized the assembly of h-BN and reduced graphite oxide (rGO) to construct h-BN/graphene-based van der Waals heterostructure nanocomposites through electrostatic interaction [86]. The ideal hybrid BN/rGO film structure is schematically illustrated in Figure 7a. Figure 7b,c present the macroscopic morphology and microstructure of the film, respectively. Through mixing and vacuum-filtering amine-modified rGO and a hydroxyl-functionalized h-BN dispersion, a BN/rGO film was acquired with a uniform multilayer architecture. It was further demonstrated that the BN/rGO film could be used as electrodes for flexible SCs with excellent structural flexibility. As shown in Figure 7d, the device displayed 100% capacitance retention even after 1000 bending tests, which evidences that BN in a heterostructure composite can enhance the mechanical strength of the film as a nanofiller.

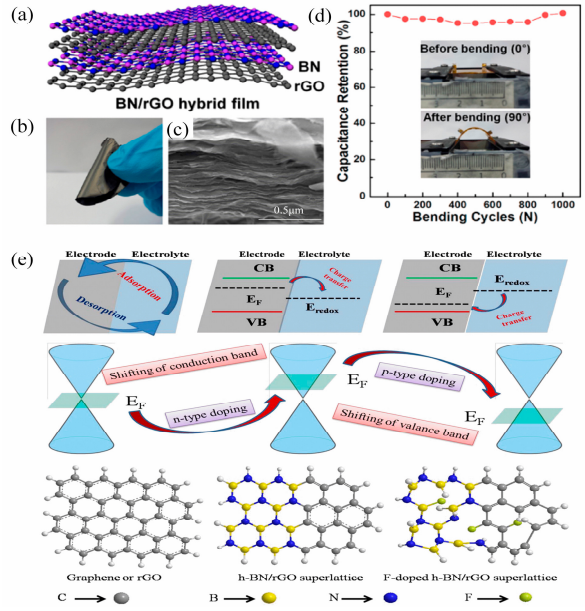

Figure 7. (**a**) Schematic illustration of the ideal BN/rGO hybrid film; (**b**) digital image and (**c**) SEM image of the hybrid film; (**d**) mechanical properties of the hybrid films. Reprinted with permission from [86]. Copyright 2016, American Chemical Society. (**e**) Illustration of the possible atomic structure, electronic band structure, and charge transfer for graphene and F-doped/undoped h-BN/rGO. Reprinted with permission from [87]. Copyright 2018, Elsevier.

Zheng et al. reported a well-constructed h-BN/graphene heterostructure material which showed a maximum capacitance of 134 F g^{-1} and excellent cycling stability (~96% retention @ 10,000 cycles at 10 A g^{-1}) based on the liquid-phase exfoliation method [88]. Pati et al. fabricated a 2D/3D heterostructure material of h-BN/rGO with the maximum capacitance of 304 F g^{-1} (at 1 A g^{-1}) in alkaline conditions and a good rate capability (98% of the initial capacitance after 10,000 cycles) via a hydrothermal assembly strategy [89]. Saha et al. elaborately investigated the effect of different concentrations of rGO within the hBN/graphene composite on the electrical and electrochemical properties of an h-BN/rGO heterostructure via a simple pyrolysis method [90]. It was found that increasing the rGO amount caused the transition from pseudocapacitance to EDLC and the sheet-like h-BN/rGO superlattice exhibited its highest specific capacitance of ~960 F g^{-1} at a scan rate of 10 mV s^{-1}. Saha and co-workers subsequently found that a fluorine (F)-doped h-BN/rGO superlattice exhibited a decreased bandgap (~1.79 eV) compared to the h-BN/rGO superlattice (~2.1 eV) [87]. As shown in Figure 7e, the electrochemical activity of electrode materials changes from n-type semiconductor to p-type when element doping happens. The h-BN/rGO superlattice exhibits an enhanced specific capacitance (942 F g^{-1}, 10 mV s^{-1}) compared to graphene/rGO because charge transfer occurs not only on the surface of the electrode material, but also in the interior of h-BN/rGO superlattice at specific redox potentials. Conversely, F doping triggers the shift of Fermi level towards the valance band of the electrode, that is, to a lower energy level compared with the redox potential of the electrolyte. The charge transfer of the F-doped h-BN/rGO superlattice occurs from the electrolyte to the electrode at the interface, leading to an increased capacitance (1250 F g^{-1}, 10 mV s^{-1}) in comparison to the EDLC capacitance.

Owing to the similar lattice constant with graphene, high mechanical strength, as well as the pseudocapacitive nature of h-BN, h-BN can serve as a 2D substrate and electrolyte channel in h-BN/graphene heterostructure nanocomposites, thus effectively enhancing the electrochemical performance and flexibility of supercapacitors [16]. However, the synthesis of these h-BN/graphene heterostructures always suffers from problems such as a high cost and low efficiency. The traditional micromechanical cleavage of bulk h-BN and graphite crystals can maintain the complete lattice of the parent materials while the low yield limits its practical application. The CVD method can realize the direct growth of h-BN on graphene, but the complex transfer procedure and expensive catalysts also hinder the large-scale preparation. Liquid exfoliation combined with vacuum filtering is an alternative low-cost method to fabricate such h-BN/graphene heterostructures, whereas the limitations, such as poor dispersity and the small lateral sizes of the products, still need to be solved [86]. To conquer these shortcomings, a potential effective solution is to functionalize h-BN or graphene in advance. For example, ball milling allows large-scale production of aminated or hydroxylated h-BN/graphene. Then, h-BN/graphene heterostructures can be scaled up through filtering or printing.

4.2. BCN-Based Supercapacitor

Ternary BCN materials also show improved supercapacitor behavior compared to carbon-based materials [91]. Heteroatom doping not only modifies the surface polarity, but also affects the pseudocapacitive effect of carbon materials. The specific capacitance of BCN material is 247 F g^{-1} at 2 mV s^{-1}, which is more than twice that of dopant-free carbon materials (111 F g^{-1} at 2 mV s^{-1}) [91]. As compared to h-BN/graphene heterostructures, the synthesis of BCN nanomaterials is more productive and easier to modify. In the past decade, various BCN nanomaterials have been successfully used in supercapacitor applications. For example, Iyyamperumal et al. synthesized vertically aligned BCN nanotubes (VA-BCNs) with high specific capacitance (321.0 F g^{-1}) from a single melamine diborate precursor using the CVD method [92]. Owing to the synergetic effects arising from the heteroatom doping and the well-aligned nanotube structure, VA-BCNs display a higher specific capacitance than nonaligned BCNs (167.3 F g^{-1}) and undoped multiwalled carbon nanotubes (117.3 F g^{-1}). Subsequently, Zhou et al. fabricated a high-performance electrochemical

capacitor based on vertically aligned BC_2N nanotube arrays (VA-BC_2NNTAs) via a one-step solvothermal method using $NaBH_4$, NaN_3, and hexadecyl trimethyl ammonium bromide (CTAB) as starting materials at low temperature [93]. The well-aligned nonbuckled tubular structure of VA-BC_2NNTAs means it possesses an extremely high specific capacitance (547 F g^{-1}) and maintains an excellent rate capability and durability. Dou et al. reported a BCN graphene electrode material which is prepared through the thermal annealing of graphene oxide and melamine diborate mixtures at 600–1000 °C [94]. The specific capacitance of BCN (130.7 F g^{-1} at 0.2 A g^{-1}) is nearly 1.7 times that of an undoped graphene electrode (77.4 F g^{-1}). Wu et al. prepared 3D B and N co-doped graphene aerogels (BN-GAs) in the presence of GO and ammonia boron trifluoride using a hydrothermal method, showing larger specific capacitance (62 F g^{-1}) and higher energy density (≈8.65 W h kg^{-1}) and power density (≈1600 W kg^{-1}) with respect to undoped GAs in all-solid-state supercapacitors (ASSSs) [95]. Element doping on the honeycomb structure will introduce a large number of defects in BCN materials and increase the number of active sites for electron transfer [96,97]. Wang and co-workers successfully prepared bandgap-tunable porous BCNNs using boric acid, urea, and glucose precursors by annealing and exfoliating [98]. Figure 8a schematically illustrates that the bandgap of BCNNs ranges from 5.5 to 1.0 eV as the carbon content increased. The as-prepared BCNNs possess a sheet-like morphology with a thickness of approximately 1.71 nm, as shown in Figure 8b. The as-prepared BCNNS also have massive active sites as an electrode material, resulting in an enhancement in capacitance through faradaic contributions. A possible pseudocapacitive mechanism is depicted in Figure 8c. The great binding energy between pyridinic sites with H^+ promotes positively the increase in pseudocapacitance. Due to the large SSA (600.9 m^2 g^{-1}) and good conductivity (10.8 S m^{-1}), BCNNS samples exhibit great specific capacitance (464.5 F g^{-1}), excellent cycle stability (98.5% of the initial capacitance after 10,000 cycles), and ultrahigh energy density (50.4 W h kg^{-1}, in 1 M Et_4NBF_4 electrolyte, displayed in Figure 8d). Karbhal and co-workers recently manufactured a BCN-based flexible micro-supercapacitor (MSC) by using CO_2 laser scribing [99]. The optical image, top view, and cross-section SEM images of the MSC device are displayed in Figure 8e–h, respectively. The as-fabricated BCN-based MSC device displays high specific capacitance (72 mF cm^{-2}, at a current density of 0.15 mA cm^{-2}), excellent electrochemical stability (without any sign of further decay in capacity/efficiency after 80,000 cycles), and remarkable flexibility.

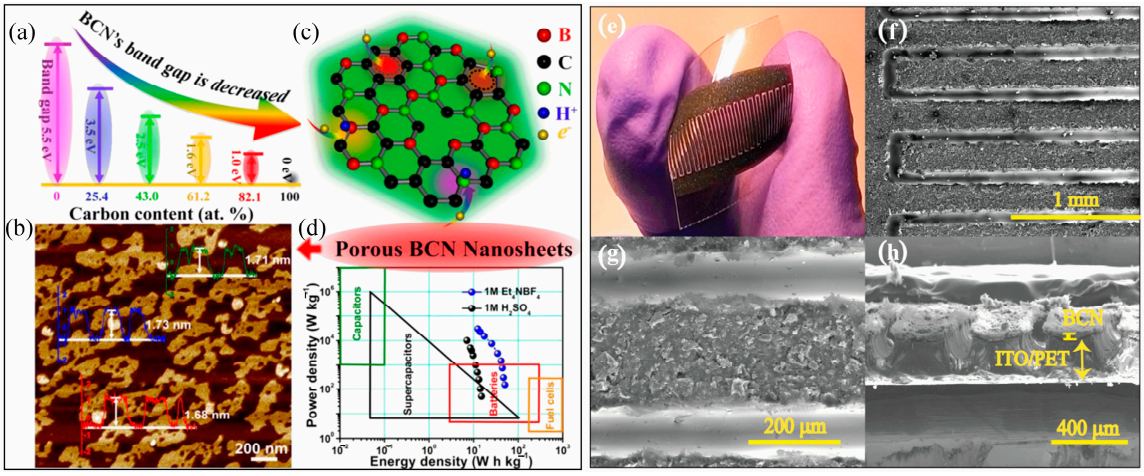

Figure 8. (**a**) Schematic illustration of the relationship between bandgap and C content of BCN; (**b**) AFM image of BCNNS; (**c**) proposed pseudocapacitive mechanism of BCN-based electrodes; (**d**) Ragone plots. Reprinted with permission from [98]. Copyright 2018, American Chemical Society. (**e**) Optical image of the device; (**f**,**g**) top view and (**h**) cross-sectional SEM images of the device. Reprinted with permission from [99]. Copyright 2021, Elsevier.

In spite of the remarkable achievements of BCN materials applied in SCs, challenges still exist to develop facile and effective approaches for the preparation of nanostructured BCN materials. Similar to the synthesis of h-BN/graphene heterostructure nanocomposites, the disadvantages such as being expensive and requiring toxic starting materials, sophisticated instruments, and laborious operations hinders the practical application of BCN materials. From the point of view of large-scale production and green synthesis, new techniques should select nontoxic, low-cost, and easily accessible raw materials. Furthermore, pre/post-processing steps should be avoided to simplify the synthesis procedure. In addition, the compositions of BCNs should be easily adjustable to determine the optimum B, C, and N source ratio. The defect sites in BCN skeletons can act as active sites for charge transfer reactions, which is beneficial for electrode materials to improve the electrochemical performance. It is important for the new synthesis techniques to prepare BCN nanomaterials with large SSA and abundant active and conductive sites.

4.3. Strategies to Boost the Electrochemical Performance of BCN-Based Supercapacitors

In recent years, many strategies such as designing and fabricating porous and defective BCN nanomaterials with diverse structures and constructing heterostructures or nanocomposites have been applied to boost the electrochemical performance of BCN-based supercapacitors [100–104]. For example, Shi et al. fabricated a BCN-polyaniline (PANI)-based electrochemical capacitor which possesses a high voltage window of 3.0 V (1 M Et_4N BF_4 as the electrolyte) and ultrahigh energy density of 67.1 W h kg^{-1} [105]. PANI modification changed the EDLC behavior and stacked-layer structure of BCNNs, providing a promising strategy to configure BCN-based composite electrodes for other energy storage devices. In this subsection, supercapacitors with three types of BCN-based nanomaterial electrodes and various building principles are briefly summarized.

4.3.1. 1D BCN-Based Electrode Materials

Owing to the structural merits, 1D BCN nanotubes/nanofibers exhibit tremendous performance for energy storage materials because the unique hollow tubular structure can effectively improve the ion diffusion channel properties of BCNNT-based SCs [106,107]. For instance, Li^+ ions can diffuse into sites either on the outer or the inner surface of hollow BCNNTs and can be inserted within the BCN layers of BCNNTs [108]. Xu et al. successfully synthesized a $Na_{0.76}V_6O_{15}$@BCNNT cathode with excellent capacity, good cyclic stability, and an energy density of 238.7 Wh kg^{-1} (at 200 W kg^{-1}) for lithium-ion capacitors (LICs) [109]. Liang et al. reported a strategy for the in situ growth of BCNNTs on carbon fibers and assembled a symmetric supercapacitor with a BCNNT electrode in a 1-ethyl-3-methylimidazolium tetrafluoroborate (EMIM·BF_4) electrolyte [110]. The 1D physical structure of BCNNTs is advantageous in maintaining the structural integrity and resisting the damage caused by the swift adsorption/desorption of the electrolyte during long-period charge/discharge cycles at high temperatures, leading to an enhancement in the high-temperature cycle stability. Benefitting from the synergy between the high conductivity of BCNNTs and the lamellar structure of MoS_2, Tu and co-workers manufactured a highly dense BCN nanofiber core with a MoS_2 shell for a high-performance supercapacitor (446.3 A g^{-1} at current density of 0.25 A g^{-1}) [111]. In short, 1D BCN materials possess large SSA, high structural stability, and excellent mechanical strength, leading to an enhanced capacitance and electrical conductivity. New advancements such as combining metal oxides, carbon fibers, and other 2D materials are regarded as efficient strategies to fabricate 1D BCN-based hybrid electrode materials for high-performance SCs. Hybridization with pseudocapacitive materials is conducive for BCN-based SC devices to enlarge their energy density values. However, it should be noted that the weak interaction between 1D BCN materials and other materials tends to cause the uneven distribution or untight contact on the BCN surface. Therefore, finding a new strategy to combine 1D BCNs with functional materials still remains a challenge.

4.3.2. 2D BCN-Based Electrode Materials

Focusing on SCs, 2D BCNNs and their nanocomposites as advanced materials have been widely used due to their large energy storage capabilities, astonishing electronic conductivity, and concomitant mechanical properties [112]. However, the inherent restacking and stability of 2D honeycomb structures hamper the further increase in capacitance. Pore/defect engineering and introducing a complementary high-performance 2D counterpart material can improve the surface area and alleviate the stability issue of both 2D materials, respectively, providing enhanced synergistic interplayed energy storage opportunities [113]. Panda et al. obtained hierarchal porous BCNNs (p-BCN) with extremely high SSA (3310.4 m^2 g^{-1}) by KOH activation at high temperatures [114]. It was found that the assembled symmetric p-BCN device possessed high energy and power densities (17 W h Kg^{-1} and 4000 W kg^{-1}) with high cycling stability. Zhang and co-workers developed a high-performance MSC using a 2D BCN nanomesh as the electrode material with pseudocapacitive charge storage capacity [115]. Figure 9a schematically illustrates the in-plane MSC configuration in which parallel integrated BCN micro-electrodes are designed and PVA/H_3PO_4 gel serves as electrolyte for on-chip energy storage applications. Figure 9b–f are the electrochemical characterizations of BCN-MSCs, which reveal that BCNN900- MSCs have the highest areal capacitance (80.1 mF cm^{-2}) and good cyclability (capacitance retention of 92% after 10,000 cycles). Shi et al. designed a BCN-assisted built-in electric field in a heterostructure and successfully broadened the voltage window of aqueous supercapacitors (1.2 V to 2 V in MnO/MnS@BCN-based symmetrical supercapacitors) by utilizing the synergistic effect [116]. Nasrin and co-workers constructed an MXene/BCN heterostructure electrode which shows a high specific capacitance of 1173 F g^{-1} (at 2 A g^{-1}) and an energy density of 45 Wh kg^{-1} [117]. Notably, the as-assembled solid-state device exhibits an ultra-high cyclability without any degradation after 100,000 cycles (100% capacitive retention).

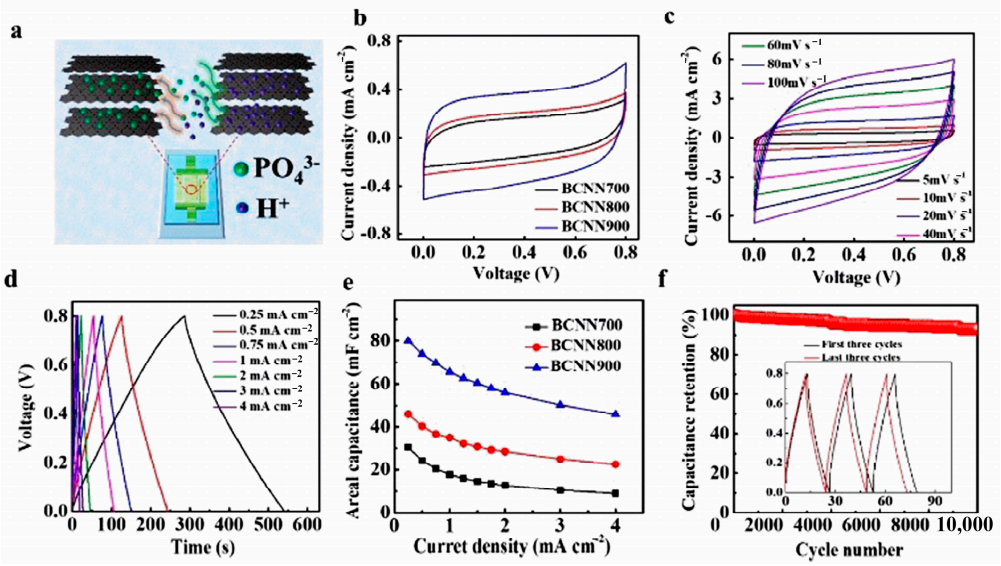

Figure 9. (**a**) Illustration of the planar structure of MSC; (**b**) CV curves obtained at a scan rate of 5 mV s^{-1} and (**c**) at scan rates ranging from 10 to 100 mV s^{-1}; (**d**) GCD plots; (**e**) areal capacitances; (**f**) cycling stability curves of BCN. Reprinted with permission from [115]. Copyright 2021, Elsevier.

BCNNs are well suited for SC applications owing to their extraordinary thermal and electrical conductivities, high SSA, excellent tensile strength and good flexibility. Unfortunately, single BCN layers tend to restack because of the interaction between adjacent BCN layers. Serious agglomeration issues will reduce the SSA and may prevent the diffusion of electrolyte ions between BCN layers. However, defects will accelerate the charge transfer reaction and an appropriate porosity may improve the electrical conductivity. Hence, it

is still a challenge and desirable to design new routes to prepare porous and defective BCN nanomaterials. In addition, coupling with other pseudocapacitive materials can also alleviate the restacking issue of BCNNs and enhance the electrochemical performance of 2D BCN-based SCs.

4.3.3. 3D BCN-Based Electrode Materials

Another alternative type of electrode material platform for the assembly of BCN-based SCs is 3D nanostructured materials. Compared with 1D and 2D nanomaterials, the infinite growth from 3D features in their spatial structure make 3D BCN-based nanomaterials possess abundant active sites and porous-and-loose characteristics, which is beneficial for supercapacitors with high capacitance performance [118,119]. Tabassum et.al reported a BCNNT architecture entangled on a 3D melamine-foam-derived carbon skeleton with high surface area and hierarchical porosity which displayed a large capacitance of 344 F g^{-1} at a current density of 1 A g^{-1} [120]. In addition, the as-prepared 3D BCN could be used as electrodes in a symmetric supercapacitor (presenting a high energy density of 19.8 W h kg^{-1} and elevated power density of 5074 W kg^{-1}) and the negative electrode in an asymmetric hybrid supercapacitor (energy density of 72 W h kg^{-1} and elevated power density of 22,732 W kg^{-1}). Zou and co-workers fabricated B, N co-doped holey graphene aerogels (BN-HGA) with an SSA of 249 m^2 g^{-1} and rich B-N motifs for flexible SCs [121]. The electrochemical characterization results of the as-assembled BCN-based SCs are shown in Figure 10a–g. The rich B-N motifs in the BN-HGA electrode cause the high surface polarity and abundant redox sites for the enhanced pseudocapacitance (a capacitance of 456 F g^{-1} at 1 A g^{-1} in three-electrode systems using sulfuric acid as electrolyte). Meanwhile, the integrated carbon matrix and the hierarchical 3D network facilitate the fast ion diffusion in the electrode and adsorption in the high-viscosity gel electrolyte, resulting in a high specific capacitance (345 mF cm^{-2} at 1 mA cm^{-2}) and outstanding rate performance (80% retention at 20 mA cm^{-2}) for all-solid-state flexible supercapacitors based on the symmetric BN-HGA electrodes. Liu et al. subsequently constructed a self-supported fluorine-doped BCN (F-BCN) aerogel material for a symmetric supercapacitor with a maximum energy density of 11.75 Wh kg^{-1} and 83% retention after 5000 charge and discharge cycles [122]. Fluorine doping leads to an increase in the defect density, expanding of the interlayer spacing, massive electrochemical active sites, and faster diffusion of ions in the electrode, thereby promoting the specific capacitance of 524.9 F g^{-1} at a specific current of 1 A g^{-1} for F-BCN. In addition, people have tried to change conventional 2D BCNNs into 3D architectures using other 2D materials. Tu and co-workers have successively achieved the assembly of 3D MXene/BCN microflowers and BCN/rGO broccoli for all-solid-state flexible MSCs with remarkable mechanical flexibility [123,124].

3D BCN materials possess a highly porous structure, eminent SSA, as well as excellent mechanical and electrical properties. The unique 3D structure of BCNs not only provides extra electron moving channels, but also offers high electrochemical performance such as large capacitance and excellent cycling stability. The template-assisted method, hydrothermal synthesis, CVD, and pyrolysis have been adopted to prepare active 3D BCN electrode materials. However, the electrical conductivity will decrease with the existence of macropores in 3D BCN, resulting in a reduction in the energy and power density values. In order to solve this problem, constructing 3D BCN-based composites with other 2D materials is an alternative to increase the accessible area for electrolyte diffusion and improve the charge transfer reaction, thus enhancing the capacitance and energy density.

The recent development of BCN-based electrodes, fabrication approaches, and their electrochemical performance as SCs are summed up in Table 2. Table 2 reveals that BCN-based electrode materials exhibit an excellent electrochemical performance through large specific capacitance, outstanding energy density, and power density in a high potential window compared to the electrolyte. Moreover, BCN-based electrodes also present good capacity retention over a long cycle, demonstrating that BCN is a promising high-performance electrode material for flexible device storage systems.

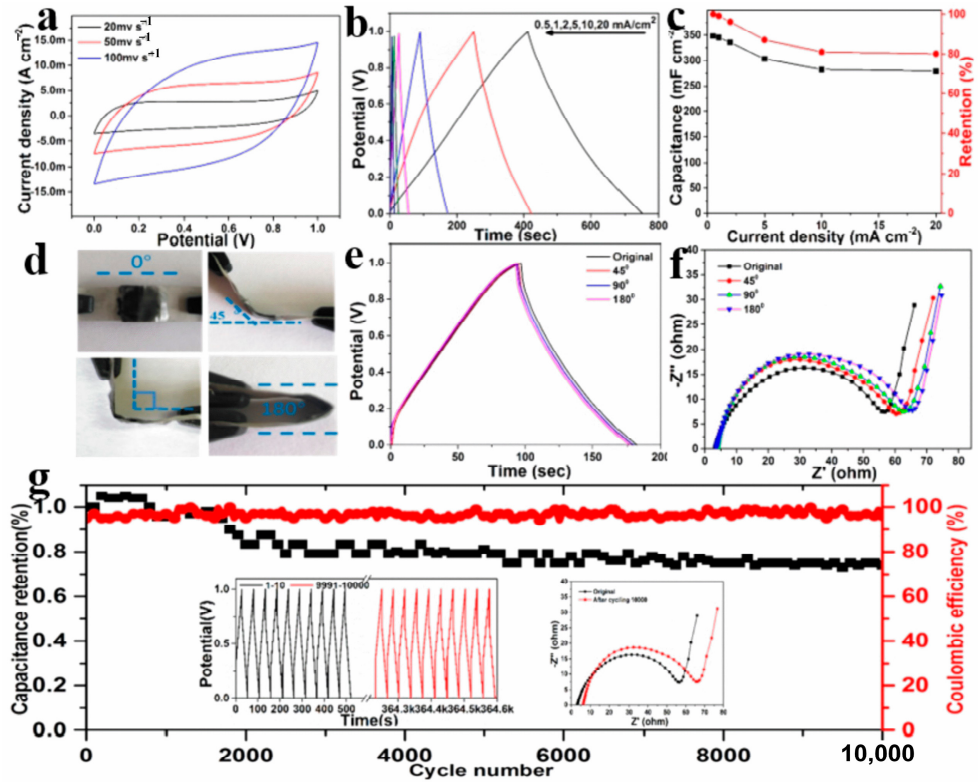

Figure 10. (**a**) CVs at scan rates ranging from 20 to 100 mV S^{-1}; (**b**) GCD plots; (**c**) capacitance and retention vs. current density; (**d**) bending images of FSC; (**e**) GCD and (**f**) EIS of the FSC; (**g**) cycling stability and coulombic efficiency at 5 mA cm^{-2}. Reprinted with permission from [121]. Copyright 2020, Elsevier.

Table 2. Performance of BCN-based electrodes in supercapacitors.

Electrode Material	Synthesis Method	Surface Area (m^2 g^{-1})	Electrolyte	Electrochemical Performance	Capacity Retention (%)	Ref.
Asymmetric supercapacitors						
h-BN/rGO heterostructure	Liquid-phase exfoliation method	371.2	2 M KOH	2.05 Wh kg^{-1}, 1998.5 W kg^{-1}	96% after 10,000 cycles at 10 A g^{-1}	[88]
h-BN/rGO superlattice	Pyrolysis	/	1 M Na_2SO_4	960 F g^{-1} @ 13 mA g^{-1}, 73 Wh kg^{-1}, 14,000 W kg^{-1}	80% after 10,000 cycles	[90]
BCN/PANI nanocomposite	In situ polymerization	146	1 M H_2SO_4	951 F g^{-1} @ 2 mVs^{-1}, 14 Wh kg^{-1}, 465 W kg^{-1}	79% after 4000 cycles	[104]
3D BCN	Template assisted pyrolysis	649	2M KOH	344 F g^{-1} @ 1 A g^{-1}, 72 W h kg^{-1}, 22,732 W kg^{-1}	80.7% after 10,000 cycles	[120]
Symmetric supercapacitors						
BCN-PANI	Ultrasonic ball milling	166.5	1 M Et_4N BF_4	3 V, 672.0 F g^{-1}@1 A g^{-1}, 67.1 W h kg^{-1}	89.6% after 10,000 cycles	[105]
BCNNT	CVD	/	1 M aqueous H_2SO_4	68.125 F g^{-1} @ 0.5 A g^{-1}, 1.51 Wh Kg^{-1}, 100 W kg^{-1}	73.6% after 1000 cycles	[107]
BCNNT	Template-assisted method	581.6	1 M EMIM·BF4	177.1 mF cm^{-2} @ 5 mA cm^{-2}, 112.5 Wh kg^{-1}, 1253.8 W kg^{-1}	86.1% after 5000 cycles	[110]
BCN/MoS_2 nanofiber	CVD	/	1 M aqueous KOH	446.3 F g^{-1} @ 0.25 A g^{-1}, 33.3 Wh kg^{-1}	91% after 5000 cycles	[111]
Porous BCNNs	Solvothermal	3310.4	1 M H_2SO_4	406 F g^{-1} under 1 A g^{-1}, 17 W h kg^{-1}, 4000 W kg^{-1}	75% after 10,000 cycles	[114]
MnO/MnS@BCN	Hydrothermal and annealing	/	1 M aqueous Li_2SO_4	2 V, 698.9 F g^{-1} @ 0.5 A g^{-1}, 75 W h kg^{-1}	75% after 10,000 cycles at 10 A g^{-1}	[116]

Table 2. *Cont.*

Electrode Material	Synthesis Method	Surface Area (m^2 g^{-1})	Electrolyte	Electrochemical Performance	Capacity Retention (%)	Ref.
BCN/MXene heterostructure	Pyrolysis	44.0	PVA/H_2SO_4 gel	1173 F g^{-1} @ 2 A g^{-1}, 45 Wh kg^{-1}	100% after 100,000 cycles	[117]
F-BCN aerogel	Hydrothermal and annealing	496.7	6 M KOH	524.9 F g^{-1} @ 1 A g^{-1}, 11.75 Wh kg^{-1}	91.4% after 10,000 cycles at 20 A g^{-1}	[122]
Micro-supercapacitors						
BCN	CO_2 laser scribing	/	PVA/H_2SO_4 gel	72 mF cm cm^{-2} @ 0.25 mA cm^{-2}	100% after 80,000 cycles	[99]
BCN nanomesh	Carbonizng gel precursor	415	PVA/H_2SO_4 gel	3.2 V, 80.1 mF cm^{-2} @ 0.25 mA cm^{-2}, 67.6 mWh cm^{-3} @ 0.8 Wh cm^{-3} (using $EMIMBF_4$/PVDF-HFP electrolyte)	92% after 10,000 cycles	[115]
BCN/MXene microflowers	Hydrothermal and sonicating	/	PVA/H_2SO_4 gel	89 mF cm^{-2} @ 0.5 mA cm^{-2}, 0.0124 mW h cm^{-2}, 3.1 mW cm^{-2}	90.1% after 10,000 cycles	[123]
3D BCN/rGO broccoli	Pyrolysis	607	PVA/H_2SO_4 gel	72.2 mF cm^{-2} @ 0.1 mA cm^{-2}, 1175 mW cm^{-2} @ 2.5 mA cm^{-2}, 11 mWh cm^{-2} @ 0.1 mA cm^{-2}	95% after 10,000 cycles	[124]

5. Conclusions and Future Outlook

This review mainly summarizes the synthesis, properties, and application of BxCyNz materials for supercapacitors. The excellent mechanical, thermal, optical, and electrical properties of h-BN and graphene can be combined and tuned in BCN nanostructures. The energy storage mechanisms, fabrication approaches, and electrochemical performances of 1D/2D/3D BCN-based SCs aimed at their structural types and parameters are also reviewed. Through taking some breakthrough work as an example, the electrochemical properties of BCN-based electrode materials have been greatly improved by optimizing their structure and composition. However, most reported studies have adopted multiple steps and complex process synthesis routes. From an energy and a manufacturing perspective, it is necessary to develop a simple, environmentally friendly, cost-effective, single-step preparation method with high yield. In addition, designing and fabricating nanostructured BCN-based materials with higher redox reactions and better pseudocapacitive behavior is an essential step for the next-generation energy storage system with further improved electrochemical performance. Herein, there are various directions for research work to carry out, i.e., morphological modification such as the formation of nanotubes/nanosheets/3D architecture and porosity development (introducing more electrochemical active sites and enlarging the SSA), heteroatom doping (n-type or p-type to enhance conductivity), construction of nanocomposite (using Faraday/Faraday materials).

Although considerable research progress on BCN-based electrode materials has been significantly promoted by scientific and rational material design, there are still several obstacles that should be addressed for the future advanced energy storage devices.

(1) It is still a challenge to synthesize semiconducting BCNs with both high electric conductivity and pseudocapacitive performance. The most advanced technique for synthesizing BCN nanomaterials is still lacking. To tune the electrochemical properties of BCN materials, advanced synthesis techniques, i.e., constructing unique structures such as vertically aligned BCN nanotube arrays, 2D porous nanosheets, and 3D hierarchical 3D networks, and controlling the BCN compositions by varying the combinations of starting materials, and designing novel synthesis routes, are required.
(2) The electron and ion transport properties of BCNs should be further increased during the electrochemical processes. The restacking and irreversible agglomeration issues may damage the porous structure of BCNs, influencing the charge transportation

and electrolyte access to the BCN surface. Functionalized BCN materials are efficient in inhibiting restacking of BCN layers and introducing more defect sites in BCN skeletons. The methods of functionalization include doping and coupling with other functional materials. Diverse functional materials such as metal oxides, conductive polymers, carbon materials, and other 2D materials can be used to improve the capacitance, energy, and power density of BCNs. Doping with heteroatoms such as F and S can also change the electrical properties of BCNs.

(3) Constructing BCN-based heterostructures is an alternative while the weak interaction forces in the hybrid structure are adverse for the interface stability during charging and discharging. Heterostructures can alleviate the restacking of BCN and enhance the electrical conductivity of nanocomposites. To make these materials viable, graphene, Mxenem and other 2D materials can be incorporated via strong π-π stacking or weak van der Waals interactions. A stronger bonding heterostructure should be considered for follow-up research work.

(4) Additionally, the feasibility of BCN preparation on an industrial scale, the longer time/cycles to maintain high performance and flexibility, and electrolyte selection will all affect the electrochemical properties and the commercialization of BCN electrode materials.

In summary, despite the abovementioned challenges, the porous structure, enhanced surface area, abundant electrochemical active sites, and unique electrical properties of BCN nanomaterials make them very promising for supercapacitor applications. Explicitly, creating new ideas, adopting new nanoscience technology to create innovative materials, and studying their structural composition for ingredient optimization with substantial efforts are essential for high-performance BCN-based electrode materials.

Author Contributions: F.L.: writing—original manuscript preparation, review, and editing; X.Z.: review and editing; P.S.: editing; Q.D.: editing; M.T.: editing; L.L.: supervision, review, and editing; Y.W.: supervision, project administration, funding acquisition, review, and editing; and X.S.: supervision, validation, review, and editing. All authors have read and agreed to the published version of the manuscript.

Funding: The present work was supported by the National Natural Science Foundation of China (grant no. 51974188), and the Liaoning Revitalization Talents Program (no. XLYC2008014).

Data Availability Statement: Data sharing is not applicable to this article.

Conflicts of Interest: Authors declare that there is no conflict of interest for this publication.

References

1. Zhao, X.; Li, H.; Zhang, M.; Pan, W.; Luo, Z.; Sun, X. Hierarchical nanocages assembled by NiCo-layered double hydroxide nanosheets for a high-performance hybrid supercapacitor. *ACS Appl. Mater. Interfaces* **2022**, *14*, 34781–34792. [CrossRef] [PubMed]
2. Zhao, X.; Zhang, M.; Li, H.; Pan, W.; Luo, Z.; Sun, X. Smart construction of $MnCo_2O_4$ microspheres with multiple interiors: Morphological evolution and structure-performance relationship for supercapacitor electrodes. *Appl. Surf. Sci.* **2022**, *600*, 154062. [CrossRef]
3. Karbhal, I.; Chaturvedi, V.; Patrike, A.; Yadav, P.; Shelke, M.V. Honeycomb boron carbon nitride as high-performance anode material for Li-ion batteries. *ChemNanoMat* **2022**, *8*, e202200056. [CrossRef]
4. Panchatcharam, P.; Vengidusamy, N.; Arumainathan, S. Facile in situ synthesis of flexible porous polycarbazole/BCN nanocomposite as a novel electrode material for high-performance supercapacitor. *J. Mater. Sci. Mater. Electron.* **2022**, *33*, 23580–23598. [CrossRef]
5. Karthikeyan, S.; Narenthiran, B.; Sivanantham, A.; Bhatlu, L.D.; Maridurai, T. Supercapacitor: Evolution and review. *Mater. Today Proc.* **2021**, *46*, 3984–3988. [CrossRef]
6. Kumar, S.; Saeed, G.; Zhu, L.; Hui, K.N.; Kim, N.H.; Lee, J.H. 0D to 3D carbon-based networks combined with pseudocapacitive electrode material for high energy density supercapacitor: A review. *Chem. Eng. J.* **2021**, *403*, 126352. [CrossRef]
7. Al-Enizi, A.M. Waste cigarette butt-derived B, N doped bifunctional hierarchical mesoporous carbon for supercapacitor and oxygen reduction reaction. *Colloids Surf. A* **2022**, *643*, 128775. [CrossRef]
8. Yang, L.; Wu, D.; Wang, T.; Jia, D. B/N-codoped carbon nanosheets derived from the self-assembly of chitosan–amino acid gels for greatly improved supercapacitor performances. *ACS Appl. Mater. Interfaces* **2020**, *12*, 18692–18704. [CrossRef]

9. Pu, J.; Zhang, K.; Wang, Z.; Li, C.; Zhu, K.; Yao, Y.; Hong, G. Synthesis and modification of boron nitride nanomaterials for electrochemical energy storage: From theory to application. *Adv. Funct. Mater.* **2021**, *31*, 2106315. [CrossRef]
10. Shan, Q.; Ding, Q.; Wang, X.; Wu, W. Electrochemical preparation of hydroxylated boron nitride nanosheets for solid–state flexible supercapacitors using deep eutectic solvent and water mixture as electrolytes. *Langmuir* **2022**, *38*, 8169–8178. [CrossRef]
11. Nasrin, K.; Sudharshan, V.; Subramani, K.; Sathish, M. Insights into 2D/2D MXene heterostructures for improved synergy in structure toward next-generation supercapacitors: A review. *Adv. Funct. Mater.* **2022**, *32*, 2110267. [CrossRef]
12. Chang, C.; Chen, W.; Chen, Y.; Chen, Y.; Chen, Y.; Ding, F.; Fan, C.; Fan, H.; Fan, Z.; Gong, C.; et al. Recent progress on two-dimensional materials. *Acta Phys.-Chim. Sin.* **2021**, *37*, 2108017. [CrossRef]
13. Nahirniak, S.; Ray, A.; Saruhan, B. Challenges and future prospects of the mxene-based materials for energy storage applications. *Batteries* **2023**, *9*, 126. [CrossRef]
14. Liang, C.; Wang, S.; Sha, S.; Lv, S.; Wang, G.; Wang, B.; Li, Q.; Yu, J.; Xu, X.; Zhang, L. Novel semiconductor materials for advanced supercapacitors. *J. Mater. Chem. C* **2023**, *11*, 4288–4317. [CrossRef]
15. Maity, C.K.; Sahoo, S.; Verma, K.; Behera, A.K.; Nayak, G.C. Facile functionalization of boron nitride (BN) for the development of high-performance asymmetric supercapacitors. *New J. Chem.* **2020**, *44*, 8106–8119. [CrossRef]
16. Althubaiti, N.; Mussa, Y.; Bongu, C.S.; Bayhan, Z.; Arsalan, M.; Soliman, A.; Alsharaeh, E. Reduced graphene oxide/hexagonal boron nitride-based composite as a positive electrode in asymmetric supercapacitors. *J. Mater. Sci.* **2022**, *57*, 14371–14385. [CrossRef]
17. Karbhal, I.; Devarapalli, R.R.; Debgupta, J.; Pillai, V.K.; Ajayan, P.M.; Shelke, M.V. Facile green synthesis of bcn nanosheets as high-performance electrode material for electrochemical energy storage. *Chem.-Eur. J.* **2016**, *22*, 7134–7140. [CrossRef]
18. Kaur, M.; Singh, K.; Vij, A.; Kumar, A. Recent insight into BCN nanomaterials–synthesis, properties and applications. *New J. Chem.* **2023**, *47*, 2137–2160. [CrossRef]
19. Han, R.; Liu, F.; Wang, X.; Huang, M.; Li, W.; Yamauchi, Y.; Sun, X.; Huang, Z. Functionalised hexagonal boron nitride for energy conversion and storage. *J. Mater. Chem. A* **2020**, *8*, 14384–14399. [CrossRef]
20. Sathish, C.I.; Kothandam, G.; Selvarajan, P.; Lei, Z.; Lee, J.; Qu, J.; Al-Muhtaseb, A.H.; Yu, X.; Zheng, R.; Vinu, A.; et al. Ordered mesoporous boron carbon nitrides with tunable mesopore nanoarchitectonics for energy storage and CO_2 adsorption properties. *Adv. Sci.* **2022**, *9*, 2105603. [CrossRef]
21. Rao, C.N.R.; Chhetri, M. Borocarbonitrides as metal-free catalysts for the hydrogen evolution reaction. *Adv. Mater.* **2019**, *31*, 1803668. [CrossRef] [PubMed]
22. Singh, N.K.; Pramoda, K.; Gopalakrishnan, K.; Rao, C.N.R. Synthesis, characterization, surface properties and energy device characterstics of 2D borocarbonitrides, (BN)xC1x, covalently cross-linked with sheets of other 2D materials. *RSC Adv.* **2018**, *8*, 17237–17253. [CrossRef] [PubMed]
23. Garg, H.; Patial, S.; Raizada, P.; Nguyen, V.H.; Kim, S.Y.; Van Le, Q.; Ahamad, T.; Alshehri, S.M.; Hussain, C.M.; Singh, P.; et al. Hexagonal-borocarbonitride (h-BCN) based heterostructure photocatalyst for energy and environmental applications: A review. *Chemosphere* **2022**, *313*, 137610. [CrossRef]
24. Recepoglu, Y.K.; Goren, A.Y.; Vatanpour, V.; Yoon, Y.; Khataee, A. Boron carbon nitride nanosheets in water and wastewater treatment: A critical review. *Desalination* **2022**, *533*, 115782. [CrossRef]
25. Rao, C.N.R.; Gopalakrishnan, K. Borocarbonitrides, BxCyNz: Synthesis, Characterization, and Properties with potential applications. *ACS Appl. Mater. Interfaces* **2017**, *9*, 19478–19494. [CrossRef]
26. Bahadur, R.; Singh, G.; Bando, Y.; Vinu, A. Advanced porous borocarbonitride nanoarchitectonics: Their structural designs and applications. *Carbon* **2022**, *190*, 142–169. [CrossRef]
27. Nehate, S.D.; Saikumar, A.K.; Prakash, A.; Sundaram, K.B. A review of boron carbon nitride thin films and progress in nanomaterials. *Mater. Today Adv.* **2020**, *8*, 100106. [CrossRef]
28. Fan, M.; Wu, J.; Yuan, J.; Deng, L.; Zhong, N.; He, L.; Cui, J.; Wang, Z.; Behera, S.K.; Zhang, C.; et al. Doping nanoscale graphene domains improves magnetism in hexagonal boron nitride. *Adv. Mater.* **2019**, *31*, 1805778. [CrossRef]
29. Chen, S.; Chen, Z.; Siahrostami, S.; Higgins, D.; Nordlund, D.; Sokaras, D.; Kim, T.R.; Liu, Y.; Yan, X.; Nilsson, E.; et al. Designing boron nitride islands in carbon materials for efficient electrochemical synthesis of hydrogen peroxide. *J. Am. Chem. Soc.* **2018**, *140*, 7851–7859. [CrossRef]
30. Yi, K.; Jin, Z.; Bu, S.; Wang, D.; Liu, D.; Huang, Y.; Dong, Y.; Yuan, Q.; Liu, Y.; Wei, D.; et al. Catalyst-free growth of two-dimensional bcxn materials on dielectrics by temperature-dependent plasma-enhanced chemical vapor deposition. *ACS Appl. Mater. Interfaces* **2020**, *12*, 33113–33120. [CrossRef]
31. Liu, F.; Nattestad, A.; Naficy, S.; Han, R.; Casillas, G.; Angeloski, A.; Sun, X.; Huang, Z. Fluorescent carbon-and oxygen-doped hexagonal boron nitride powders as printing ink for anticounterfeit applications. Adv. *Opt. Mater.* **2019**, *7*, 1901380. [CrossRef]
32. Liu, F.; Han, R.; Nattestad, A.; Sun, X.; Huang, Z. Carbon-and oxygen-doped hexagonal boron nitride for degradation of organic pollutants. *Surf. Innov.* **2020**, *9*, 222–230. [CrossRef]
33. Liu, F.; Han, R.; Zhang, G.; Zhang, M.; Chen, J.; Sun, X. Molten salt assisted synthesis of boron carbon nitride nanosheets for enhanced photocatalytic activity of silver phosphate. *J. Nanoelectron. Optoelectron.* **2022**, *17*, 560–568. [CrossRef]
34. Kaner, R.B.; Kouvetakis, J.; Warble, C.E.; Sattler, M.L.; Bartlett, N. Boron-carbon-nitrogen materials of graphite-like structure. *Mater. Res. Bull.* **1987**, *22*, 399–404. [CrossRef]

35. Ci, L.; Song, L.; Jin, C.; Jariwala, D.; Wu, D.; Li, Y.; Srivastava, A.; Wang, A.F.; Storr, K.; Balicas, L.; et al. Atomic layers of hybridized boron nitride and graphene domains. *Nat. Mater.* **2010**, *9*, 430–435. [CrossRef] [PubMed]
36. Son, M.; Lim, H.; Hong, M.; Choi, H.C. Direct growth of graphene pad on exfoliated hexagonal boron nitride surface. *Nanoscale* **2011**, *3*, 3089–3093. [CrossRef] [PubMed]
37. Qin, L.; Yu, J.; Kuang, S.; Xiao, C.; Bai, X. Few-atomic-layered boron carbonitride nanosheets prepared by chemical vapor deposition. *Nanoscale* **2012**, *4*, 120–123. [CrossRef]
38. Roy, S.; Zhang, X.; Puthirath, A.B.; Meiyazhagan, A.; Bhattacharyya, S.; Rahman, M.M.; Babu, G.; Susarla, S.; Saju, S.K.; Tran, M.K.; et al. Structure, properties and applications of two-dimensional hexagonal boron nitride. *Adv. Mater.* **2021**, *33*, 2101589. [CrossRef]
39. Yang, W.; Chen, G.; Shi, Z.; Liu, C.C.; Zhang, L.; Xie, G.; Cheng, M.; Wang, D.; Yang, R.; Shi, D.; et al. Epitaxial growth of single-domain graphene on hexagonal boron nitride. *Nat. Mater.* **2013**, *12*, 792–797. [CrossRef]
40. Tang, S.; Wang, H.; Wang, H.S.; Sun, Q.; Zhang, X.; Cong, C.; Xie, H.; Liu, X.; Zhou, X.; Huang, F.; et al. Silane-catalysed fast growth of large single-crystalline graphene on hexagonal boron nitride. *Nat. Commun.* **2015**, *6*, 6499. [CrossRef]
41. Seo, T.H.; Lee, W.; Lee, K.S.; Hwang, J.Y.; Son, D.I.; Ahn, S.; Cho, H.; Kim, M.J. Dominant formation of h-BC_2N in h-BxCyNz films: CVD synthesis and characterization. *Carbon* **2021**, *182*, 791–798. [CrossRef]
42. Han, W.; Bando, Y.; Kurashima, K.; Sato, T. Synthesis of boron nitride nanotubes from carbon nanotubes by a substitution reaction. *Appl. Phys. Lett.* **1998**, *73*, 3085–3087. [CrossRef]
43. Han, W.Q.; Mickelson, W.; Cumings, J.; Zettl, A. Transformation of BxCyNz nanotubes to pure BN nanotubes. *Appl. Phys. Lett.* **2002**, *81*, 1110–1112. [CrossRef]
44. Kumar, N.; Subrahmanyam, K.S.; Chaturbedy, P.; Raidongia, K.; Govindaraj, A.; Hembram, K.P.; Mishra, A.K.; Waghmare, U.V.; Rao, C.N.R. Remarkable uptake of CO_2 and CH_4 by graphene-like borocarbonitrides, BxCyNz. *ChemSusChem* **2011**, *4*, 1662–1670. [CrossRef] [PubMed]
45. Liu, F.; Mo, X.; Gan, H.; Guo, T.; Wang, X.; Chen, B.; Chen, J.; Deng, S.; Xu, N.; Sekiguchi, T. Cheap, gram-scale fabrication of BN nanosheets via substitution reaction of graphite powders and their use for mechanical reinforcement of polymers. *Sci. Rep.* **2014**, *4*, 4211. [CrossRef]
46. Vinu, A.; Terrones, M.; Golberg, D.; Hishita, S.; Ariga, K.; Mori, T. Synthesis of mesoporous BN and BCN exhibiting large surface areas via templating methods. *Chem. Mater.* **2005**, *17*, 5887–5890. [CrossRef]
47. Zhang, Y.; Wang, G.; Wang, S.; Wang, J.; Qiu, J. Boron-nitride-carbon nanosheets with different pore structure and surface properties for capacitive deionization. *J. Colloid Interface Sci.* **2019**, *552*, 604–612. [CrossRef]
48. Luo, Z.; Fang, Y.; Zhou, M.; Wang, X. A borocarbonitride ceramic aerogel for photoredox catalysis. *Angew. Chem. Int. Ed.* **2019**, *58*, 6033–6037. [CrossRef]
49. Portehault, D.; Giordano, C.; Gervais, C.; Senkovska, I.; Kaskel, S.; Sanchez, C.; Antonietti, M. High-surface-area nanoporous boron carbon nitrides for hydrogen storage. *Adv. Funct. Mater.* **2010**, *20*, 1827–1833. [CrossRef]
50. Wang, S.; Wang, G.; Wu, T.; Zhang, Y.; Zhan, F.; Wang, Y.; Wang, J.; Fu, Y.; Qiu, J. BCN nanosheets templated by gC_3N_4 for high performance capacitive deionization. *J. Mater. Chem. A* **2018**, *6*, 14644–14650. [CrossRef]
51. Li, J.; Lei, N.; Hao, H.; Zhou, J. A series of BCN nanosheets with enhanced photoelectrochemical performances. *Chem. Phys. Lett.* **2017**, *672*, 99–104. [CrossRef]
52. Cao, L.; Dai, P.; Tang, J.; Li, D.; Chen, R.; Liu, D.; Gu, X.; Li, L.; Bando, Y.; Ok, Y.S.; et al. Spherical superstructure of boron nitride nanosheets derived from boron-containing metal–organic frameworks. *J. Am. Chem. Soc.* **2020**, *142*, 8755–8762. [CrossRef] [PubMed]
53. Wang, X.; Han, C.; Li, H.; Su, P.; Ta, N.; Ma, Y.; Huang, Z.; Liu, J. Fabrication of monodispersed B, N co-doped hierarchical porous carbon nanocages through confined etching to boost electrocatalytic oxygen reduction. *Nano Res.* **2023**, *16*, 290–298. [CrossRef]
54. Lu, L.; He, J.; Wu, P.; Wu, Y.; Chao, Y.; Li, H.; Tao, D.; Fan, L.; Li, H.; Zhu, W. Taming electronic properties of boron nitride nanosheets as metal-free catalysts for aerobic oxidative desulfurization of fuels. *Green Chem.* **2018**, *20*, 4453–4460. [CrossRef]
55. Goyal, R.; Sarkar, B.; Bag, A.; Lefebvre, F.; Sameer, S.; Pendem, C.; Bordoloi, A. Single-step synthesis of hierarchical BxCN: A metal-free catalyst for low-temperature oxidative dehydrogenation of propane. *J. Mater. Chem. A* **2016**, *4*, 18559–18569. [CrossRef]
56. Massimi, L.; Betti, M.G.; Caramazza, S.; Postorino, P.; Mariani, C.; Latini, A.; Leardini, F. In-vacuum thermolysis of ethane 1, 2-diamineborane for the synthesis of ternary borocarbonitrides. *Nanotechnology* **2016**, *27*, 435601. [CrossRef]
57. Zhang, P.; Hou, C.; Shao, W.; Liu, R.; Wu, Z.; Tai, G. Crystalline BC_2N quantum dots. *Nano Res.* **2023**, *16*, 7837–7843. [CrossRef]
58. Giusto, P.; Arazoe, H.; Cruz, D.; Lova, P.; Heil, T.; Aida, T.; Antonietti, M. Boron carbon nitride thin films: From disordered to ordered conjugated ternary materials. *J. Am. Chem. Soc.* **2020**, *142*, 20883–20891. [CrossRef]
59. Han, R.; Diao, J.; Kumar, S.; Lyalin, A.; Taketsugu, T.; Casillas, G.; Richardson, C.; Liu, F.; Yoon, C.W.; Liu, H.; et al. Boron nitride for enhanced oxidative dehydrogenation of ethylbenzene. *J. Energy Chem.* **2021**, *57*, 477–484. [CrossRef]
60. Mirzaee, M.; Rashidi, A.; Zolriasatein, A.; Abadchi, M.R. Solid-state synthesis and characterization of two-dimensional hexagonal BCN nanosheet using a free template method. *Diam. Relat. Mater.* **2021**, *115*, 108350. [CrossRef]
61. Huang, C.; Chen, C.; Zhang, M.; Lin, L.; Ye, X.; Lin, S.; Antonietti, M.; Wang, X. Carbon-doped BN nanosheets for metal-free photoredox catalysis. *Nat. Commun.* **2015**, *6*, 7698. [CrossRef] [PubMed]

62. Wang, J.; Hao, J.; Liu, D.; Qin, S.; Portehault, D.; Li, Y.; Chen, Y.; Lei, W. Porous boron carbon nitride nanosheets as efficient metal-free catalysts for the oxygen reduction reaction in both alkaline and acidic solutions. *ACS Energy Lett.* **2017**, *2*, 306–312. [CrossRef]
63. Tabassum, H.; Zou, R.; Mahmood, A.; Liang, Z.; Guo, S. A catalyst-free synthesis of B, N co-doped graphene nanostructures with tunable dimensions as highly efficient metal free dual electrocatalysts. *J. Mater. Chem. A* **2016**, *4*, 16469–16475. [CrossRef]
64. Tabassum, H.; Zou, R.; Mahmood, A.; Liang, Z.; Wang, Q.; Zhang, H.; Gao, S.; Qu, C.; Guo, W.; Guo, S. A universal strategy for hollow metal oxide nanoparticles encapsulated into B/N Co-doped graphitic nanotubes as high-performance lithium-ion battery anodes. *Adv. Mater.* **2018**, *30*, 1705441. [CrossRef]
65. Zhang, X.; Yan, P.; Xu, J.; Li, F.; Herold, F.; Etzold, B.J.; Wang, p.; Su, D.; Lin, S.; Qi, W.; et al. Methanol conversion on borocarbonitride catalysts: Identification and quantification of active sites. *Sci. Adv.* **2020**, *6*, eaba5778. [CrossRef]
66. Tian, L.; Li, J.; Liang, F.; Chang, S.; Zhang, H.; Zhang, M.; Zhang, S. Facile molten salt synthesis of atomically thin boron nitride nanosheets and their co-catalytic effect on the performance of carbon nitride photocatalyst. *J. Colloid Interface Sci.* **2019**, *536*, 664–672. [CrossRef]
67. Liu, F.; Han, R.; Naficy, S.; Casillas, G.; Sun, X.; Huang, Z. Few-layered boron nitride nanosheets for strengthening polyurethane hydrogels. *ACS Appl. Nano Mater.* **2021**, *4*, 7988–7994. [CrossRef]
68. Wang, L.; Wang, Y.; Zhang, R.; Ding, R.; Chen, X.; Lv, B. Edge-activating CO_2-mediated ethylbenzene dehydrogenation by a hierarchical porous BN catalyst. *ACS Catal.* **2020**, *10*, 6697–6706. [CrossRef]
69. Lei, W.; Portehault, D.; Dimova, R.; Antonietti, M. Boron carbon nitride nanostructures from salt melts: Tunable water-soluble phosphors. *J. Am. Chem. Soc.* **2011**, *133*, 7121–7127. [CrossRef]
70. Huang, L.; Hu, Z.; Jin, H.; Wu, J.; Liu, K.; Xu, Z.; Wan, J.; Zhou, H.; Duan, J.; Hu, B.; et al. Salt-assisted synthesis of 2D materials. *Adv. Funct. Mater.* **2020**, *30*, 1908486. [CrossRef]
71. Sun, Q.; Zhu, S.; Shen, Z.; Liu, Y.; Wu, C.; Kang, L.; Yang, Y. Molten-salt assisted synthesis of two-dimensional materials and energy storage application. *Mater. Today Chem.* **2023**, *29*, 101419. [CrossRef]
72. Liu, X.; Fechler, N.; Antonietti, M. Salt melt synthesis of ceramics, semiconductors and carbon nanostructures. *Chem. Soc. Rev.* **2013**, *42*, 8237–8265. [CrossRef] [PubMed]
73. Jing, H.; Ouyang, H.; Li, W.; Long, Y. Molten salt synthesis of BCNO nanosheets for the electrochemical detection of clenbuterol. *Microchem. J.* **2022**, *178*, 107359. [CrossRef]
74. Zhang, M.; Zhou, M.; Luo, Z.; Zhang, J.; Wang, S.; Wang, X. Molten salt assisted assembly growth of atomically thin boron carbon nitride nanosheets for photocatalytic H_2 evolution. *Chem. Commun.* **2020**, *56*, 2558–2561. [CrossRef]
75. Wang, H.; Tian, L.; Huang, Z.; Liang, F.; Guan, K.; Jia, Q.; Zhang, H.; Zhang, S. Molten salt synthesis of carbon-doped boron nitride nanosheets with enhanced adsorption performance. *Nanotechnology* **2020**, *31*, 505606. [CrossRef]
76. Huang, F.L.; Cao, C.B.; Xiang, X.; Lv, R.T.; Zhu, H.S. Synthesis of hexagonal boron carbonitride phase by solvothermal method. *Diam. Relat. Mater.* **2004**, *13*, 1757–1760. [CrossRef]
77. Shi, D.; Yang, M.; Chang, B.; Ai, Z.; Zhang, K.; Shao, Y.; Wang, S.; Wu, Y.; Hao, X. Ultrasonic-ball milling: A novel strategy to prepare large-size ultrathin 2d materials. *Small* **2020**, *16*, 1906734. [CrossRef]
78. Li, X.; Hao, X.; Zhao, M.; Wu, Y.; Yang, J.; Tian, Y.; Qian, G. Exfoliation of hexagonal boron nitride by molten hydroxides. *Adv. Mater.* **2013**, *25*, 2200–2204. [CrossRef]
79. Li, T.; Jiao, X.; You, T.; Dai, F.; Zhang, P.; Yu, F.; Hu, L.; Ding, L.; Zhang, L.; Wen, Z.; et al. Hexagonal boron nitride nanosheet/carbon nanocomposite as a high-performance cathode material towards aqueous asymmetric supercapacitors. *Ceram. Int.* **2019**, *45*, 4283–4289. [CrossRef]
80. Özçelik, V.O.; Ciraci, S. Nanoscale dielectric capacitors composed of graphene and boron nitride layers: A first-principles study of high capacitance at nanoscale. *J. Phys. Chem. C* **2013**, *117*, 15327–15334. [CrossRef]
81. Saha, S.; Jana, M.; Khanra, P.; Samanta, P.; Koo, H.; Murmu, N.C.; Kuila, T. Band gap engineering of boron nitride by graphene and its application as positive electrode material in asymmetric supercapacitor device. *ACS Appl. Mater. Interfaces* **2015**, *7*, 14211–14222. [CrossRef]
82. Saha, S.; Samanta, P.; Murmu, N.C.; Kim, N.H.; Kuila, T.; Lee, J.H. Electrochemical functionalization and in-situ deposition of the SAA@ rGO/h-BN@ Ni electrode for supercapacitor applications. *J. Ind. Eng. Chem.* **2017**, *52*, 321–330. [CrossRef]
83. Jia, H.; Qiu, M.; Tang, C.; Liu, H.; Fu, S.; Zhang, X. Nano-scale BN interface for ultra-stable and wide temperature range tolerable Zn anode. *EcoMat* **2022**, *4*, e12190. [CrossRef]
84. Paul, R.; Roy, A.K. BN-codoped CNT based nanoporous brushes for all-solid-state flexible supercapacitors at elevated temperatures. *Electrochim. Acta* **2021**, *365*, 137345. [CrossRef]
85. Wang, J.; Zhao, R.; Liu, Z.; Liu, Z. Widely tunable carrier mobility of boron nitride-embedded graphene. *Small* **2013**, *9*, 1373–1378. [CrossRef]
86. Byun, S.; Kim, J.H.; Song, S.H.; Lee, M.; Park, J.J.; Lee, G.; Hong, S.H.; Lee, D. Ordered, scalable heterostructure comprising boron nitride and graphene for high-performance flexible supercapacitors. *Chem. Mater.* **2016**, *28*, 7750–7756. [CrossRef]
87. Saha, S.; Samanta, P.; Murmu, N.C.; Banerjee, A.; Ganesh, R.S.; Inokawa, H.; Kuila, T. Modified electrochemical charge storage properties of h-BN/rGO superlattice through the transition from n to p type semiconductor by fluorine doping. *Chem. Eng. J.* **2018**, *339*, 334–345. [CrossRef]

88. Zheng, X.; Wang, G.; Huang, F.; Liu, H.; Gong, C.; Wen, S.; Hu, Y.; Zheng, G.; Chen, D. Liquid phase exfoliated hexagonal boron nitride/graphene heterostructure based electrode toward asymmetric supercapacitor application. *Front. Chem.* **2019**, *7*, 544. [CrossRef]
89. Patil, I.M.; Kapse, S.; Parse, H.; Thapa, R.; Andersson, G.; Kakade, B. 2D/3D heterostructure of h-BN/reduced graphite oxide as a remarkable electrode material for supercapacitor. *J. Power Sources* **2020**, *479*, 229092. [CrossRef]
90. Saha, S.; Jana, M.; Samanta, P.; Murmu, N.C.; Kim, N.H.; Kuila, T.; Lee, J.H. Investigation of band structure and electrochemical properties of h-BN/rGO composites for asymmetric supercapacitor applications. *Mater. Chem. Phys.* **2017**, *190*, 153–165. [CrossRef]
91. Guo, H.; Gao, Q. Boron and nitrogen co-doped porous carbon and its enhanced properties as supercapacitor. *J. Power Sources* **2009**, *186*, 551–556. [CrossRef]
92. Iyyamperumal, E.; Wang, S.; Dai, L. Vertically aligned BCN nanotubes with high capacitance. *ACS Nano* **2012**, *6*, 5259–5265. [CrossRef]
93. Zhou, J.; Li, N.; Gao, F.; Zhao, Y.; Hou, L.; Xu, Z. Vertically-aligned BCN nanotube arrays with superior performance in electrochemical capacitors. *Sci. Rep.* **2014**, *4*, 6083. [CrossRef]
94. Dou, S.; Huang, X.; Ma, Z.; Wu, J.; Wang, S. A simple approach to the synthesis of BCN graphene with high capacitance. *Nanotechnology* **2015**, *26*, 045402. [CrossRef] [PubMed]
95. Wu, Z.; Winterr, A.; Chen, L.; Sun, Y.; Turchanin, A.; Feng, X.; Müllen, K. Three-dimensional nitrogen and boron co-doped graphene for high-performance all-solid-state supercapacitors. *Adv. Mater.* **2012**, *24*, 5130–5135. [CrossRef]
96. Kaur, M.; Mir, R.A.; Chauhan, I.; Singh, K.; Krishnan, U.; Kumar, M.; Devi, P.; Pandey, O.P.; Kumar, A. Defect states induced luminescence and electrochemical studies of boron carbon nitride nanosheets. *Appl. Surf. Sci.* **2021**, *559*, 149982. [CrossRef]
97. Yao, Y.; Huang, G.; Liu, Y.; Liu, Y.; Li, Y.; Han, G.; Xing, B.; Liu, Q.; Jia, J.; Zhang, C. Facile synthesis of B/N co-doped porous carbon nanosheets with high heteroatom content and electrical conductivity for excellent-performance supercapacitors. *Appl. Surf. Sci.* **2022**, *580*, 152236. [CrossRef]
98. Wang, S.; Ma, F.; Jiang, H.; Shao, Y.; Wu, Y.; Hao, X. Band gap-tunable porous borocarbonitride nanosheets for high energy-density supercapacitors. *ACS Appl. Mater. Interfaces* **2018**, *10*, 19588–19597. [CrossRef]
99. Karbhal, I.; Basu, A.; Patrike, A.; Shelke, M.V. Laser patterning of boron carbon nitride electrodes for flexible micro-supercapacitor with remarkable electrochemical stability/capacity. *Carbon* **2021**, *171*, 750–757. [CrossRef]
100. Chen, D.; Huang, Y.; Hu, X.; Li, R.; Qian, Y.; Li, D. Synthesis and characterization of "Ravine-Like" BCN compounds with high capacitance. *Materials* **2018**, *11*, 209. [CrossRef]
101. Yadav, V.K.; Chakraborty, H.; Klein, M.L.; Waghmare, U.V.; Rao, C.N. R, Defect-enriched tunability of electronic and charge-carrier transport characteristics of 2D borocarbonitride (BCN) monolayers from ab initio calculations. *Nanoscale* **2019**, *11*, 19398–19407. [CrossRef]
102. Peng, J.; Dai, X.; Huang, J.; Zeng, J.; Zheng, L.; Chen, H. High-yield preparation of B/N co-doped porous carbon nanosheets from a cross-linked boronate polymer for supercapacitor applications. *J. Energy Storage* **2023**, *59*, 106498. [CrossRef]
103. Bahadur, R.; Singh, G.; Li, M.; Chu, D.; Yi, J.; Karakoti, A.; Vinu, A. BCN nanostructures conjugated nanoporous carbon with oxygenated surface and high specific surface area for enhanced CO_2 capture and supercapacitance. *Chem. Eng. J.* **2023**, *460*, 141793. [CrossRef]
104. Krishnaiah, P.; Prasanna, B.P.; Kumar, K.Y.; Asha, P.K.; Nautiyal, P.; Devi, V.S.; Alharthi, F.A.; PhD, L.P.; PhD, M.S. Fabrication of anode material for asymmetric supercapacitor device using polyaniline wrapped boroncarbonitride nanocomposite with enhanced capacitance. *J. Alloys Compd.* **2020**, *848*, 156602. [CrossRef]
105. Shi, D.; Yang, M.; Zhang, B.; Hu, H.; Ai, Z.; Shao, Y.; Shen, J.; Wu, Y.; Hao, X. Design of boron carbonitrides-polyaniline (BCN-PANI) assembled supercapacitor with high voltage window. *J. Colloid Interface Sci.* **2022**, *626*, 544–553. [CrossRef]
106. Chithaiah, P.; Pramoda, K.; Kulkarni, G.U.; Rao, C.N.R. A simple chemical route to borocarbonitride nanotubes. *Eur. J. Inorg. Chem.* **2020**, *2020*, 1230–1232. [CrossRef]
107. Devarajan, J.; Arumugam, P.; Govindasamy, G. Synthesis of BCN nanotubes by CVD method and their electrochemical performance towards supercapacitors. *Mater. Today Proc.* **2023**. [CrossRef]
108. Karbhal, I.; Chaturvedi, V.; Yadav, P.; Patrike, A.; Shelke, M.V. Template directed synthesis of boron carbon nitride nanotubes (BCN-NTs) and their evaluation for energy storage properties. *Adv. Mater. Interfaces* **2023**, *10*, 2201560. [CrossRef]
109. Xu, D.; Jiang, H.; Liang, Z.; Kong, Z.; Liu, S.; Deng, L.; Shao, Y.; Wu, Y.; Hao, X. $Na_{0.76}V_6O_{15}$@ boron carbonitride nanotube composites as cathodes for high-performance lithium-ion capacitors. *Crystals* **2022**, *12*, 597. [CrossRef]
110. Liang, Z.; Tu, H.; Shi, D.; Chen, F.; Jiang, H.; Shao, Y.; Wu, Y.; Hao, X. In situ growing BCN nanotubes on carbon fibers for novel high-temperature supercapacitor with excellent cycling performance. *Small* **2021**, *17*, 2102899. [CrossRef]
111. Tu, D.; Yang, W.; Yan, J.; Yang, Y.; Xu, J.; Chua, D.H. Highly densed BCN nanofiber core with MoS_2 shell for enhanced hydrogen evolution reaction and supercapacitance applications. *Appl. Surf. Sci.* **2023**, *615*, 156400. [CrossRef]
112. Wang, L.; Hu, P.; Long, Y.; Liu, Z.; He, X. Recent advances in ternary two-dimensional materials: Synthesis, properties and applications. *J. Mater. Chem. A* **2017**, *5*, 22855–22876. [CrossRef]
113. Hao, Y.; Wang, S.; Shao, Y.; Wu, Y.; Miao, S. High-energy density Li-ion capacitor with layered SnS_2/reduced graphene oxide anode and BCN nanosheet cathode. *Adv. Energy Mater.* **2020**, *10*, 1902836. [CrossRef]

114. Panda, P.; Samanta, R.; Barman, S. Facile synthesis of two-dimensional (2D) boron carbonitride and 2D porous boron carbonitride for excellent energy storage and gas adsorption applications. *Energy Fuels* **2023**, *37*, 5540–5555. [CrossRef]
115. Zhang, L.; Huang, K.; Wen, P.; Wang, J.; Yang, G.; Liu, D.; Lin, Z.; Lian, C.; Liu, H.; Zheng, S.; et al. Tailoring the defects of two-dimensional borocarbonitride nanomesh for high energy density micro-supercapacitor. *Energy Storage Mater.* **2021**, *42*, 430–437. [CrossRef]
116. Shi, D.; Yang, M.; Zhang, B.; Ai, Z.; Hu, H.; Shao, Y.; Shen, J.; Wu, Y.; Hao, X. BCN-assisted built-in electric field in heterostructure: An innovative path for broadening the voltage window of aqueous supercapacitor. *Adv. Funct. Mater.* **2022**, *32*, 2108843. [CrossRef]
117. Nasrin, K.; Sudharshan, V.; Subramani, K.; Karnan, M.; Sathish, M. In-situ synergistic 2D/2D MXene/BCN heterostructure for superlative energy density supercapacitor with super-long life. *Small* **2022**, *18*, 2106051. [CrossRef] [PubMed]
118. Peng, X.; Peng, L.; Wu, C.; Xie, Y. Two dimensional nanomaterials for flexible supercapacitors. *Chem. Soc. Rev.* **2014**, *43*, 3303–3323. [CrossRef] [PubMed]
119. KA, S.R.; Pramoda, K.; Rout, C.S. Assembling a high-performance asymmetric supercapacitor based on pseudocapacitive S-doped VSe_2/CNT hybrid and 2D borocarbonitride nanosheets. *J. Mater. Chem. C* **2023**, *11*, 2565–2573. [CrossRef]
120. Bassum, H.; Qu, C.; Cai, K.; Aftab, W.; Liang, Z.; Qiu, T.; Mahmood, A.; Meng, W.; Zou, R. Large-scale fabrication of BCN nanotube architecture entangled on a three-dimensional carbon skeleton for energy storage. *J. Mater. Chem. A* **2018**, *6*, 21225–21230.
121. Zou, X.; Wu, D.; Mu, Y.; Xing, L.; Zhang, W.; Gao, Z.; Xu, F.; Jiang, K. Boron and nitrogen Co-doped holey graphene aerogels with rich B-N motifs for flexible supercapacitors. *Carbon* **2020**, *159*, 94–101. [CrossRef]
122. Liu, S.; Shi, D.; Tu, H.; Yao, X.; Deng, L.; Xu, D.; Shao, Y.; Wu, Y.; Hao, X. Self-supported fluorine-doped boron carbonitride porous aerogels for high-performance supercapacitors. *Energy Technol.* **2021**, *9*, 2100824. [CrossRef]
123. Tu, D.; Yang, W.; Li, Y.; Zhou, Y.; Shi, L.; Xu, J.; Yang, Y. Three-dimensional MXene/BCN microflowers for wearable all-solid-state microsupercapacitors. *J. Mater. Chem. C* **2021**, *9*, 11104–11114. [CrossRef]
124. Tu, D.; Xu, J.; Yang, W.; Shi, L.; Chen, X.; Li, Y.; Yang, Y.; Gao, C. Synthesis of three-dimensional boron carbon nitrogen/reduced grapheme oxide broccoli as electrode material for flexible micro-supercapacitors. *Surf. Interfaces* **2022**, *30*, 101873. [CrossRef]